



1 Atmospheric H₂ observations from the NOAA Global 2 Cooperative Air Sampling Network

3 Gabrielle Pétron^{1,2}, Andrew M. Croswell^{1,2}, John Mund^{1,2}, Molly Croswell^{1,2}, Thomas Mefford^{1,2},
4 Kirk Thoning², Bradley Hall², Duane Kitzis^{1,2}, Monica Madronich^{1,2}, Eric Moglia^{1,2}, Don Neff^{1,2},
5 Sonja Wolter^{1,2}, Armin Jordan³, Paul Krummel⁴, Ray Langenfelds⁴, John Patterson⁵
6 *Correspondence to:* Gabrielle Pétron (gabrielle.petron@noaa.gov)

7

8 1. Cooperative Institute for Research in Environmental Sciences, CU Boulder, USA

9 2. NOAA Global Chemical Laboratory, Boulder, USA

10 3. Max-Planck-Institute for Biogeochemistry (MPI-BGC), Jena, Germany

11 4. Commonwealth Scientific and Industrial Research Organisation - Environment, Aspendale, Australia

12 5. Department of Earth System Science, University of California, Irvine, USA

13

14

15 **Abstract.** The NOAA Global Monitoring Laboratory measures atmospheric hydrogen (H₂) in
16 grab-samples collected weekly as flask pairs at over 50 sites in the Global Cooperative Air Sampling
17 Network. These NOAA H₂ measurements from 2009 to 2021 are publicly available. Measurements
18 representative of background air sampling show higher H₂ in recent years at all latitudes. The marine
19 boundary layer (MBL) global mean H₂ was 20.2 ± 0.2 ppb higher in 2021 compared to 2010. A 10 ppb or
20 more increase over the 2010-2021 average annual cycle was detected in 2016 for MBL zonal means in the
21 tropics and in the Southern Hemisphere. Carbon monoxide measurements in the same air samples suggest
22 large biomass burning events in different regions likely contributed to the observed interannual variability
23 at different latitudes. A major focus in recent years involved the adoption of the World Meteorological
24 Organization Global Atmospheric Watch (WMO GAW) H₂ mole fraction X2009 calibration scale,
25 developed and maintained by the Max-Planck Institute for Biogeochemistry (MPI-BGC), Jena, Germany.
26 GML maintains eight H₂ primary calibration standards to propagate the MPI scale. These are gravimetric
27 hydrogen-in-air mixtures in electropolished stainless steel cylinders (Essex Industries, St. Louis, MO)
28 which are stable for H₂. These mixtures were calibrated at the MPI-BGC, the WMO Central Calibration
29 Laboratory (CCL) for H₂, in late 2020 and span the range 250-700 ppb. We have used the CCL
30 assignments to propagate the MPI X2009 H₂ calibration scale to NOAA air measurements performed
31 using Gas Chromatography-Helium Pulse Discharge Detector instruments since 2009. To propagate the
32 scale, NOAA uses a hierarchy of secondary and tertiary standards, which are high pressure tanks with
33 whole air mixtures calibrated against the primary and secondary standards respectively. NOAA secondary
34 and tertiary standards are stored in aluminum cylinders, which have a tendency to grow H₂ over time. We
35 fit the calibration histories of these standards with 0-2nd order polynomial functions of time and use the
36 time-dependent mole fraction assignments on the MPI X2009 to reprocess all tank air and flask air
37 measurement records. The robustness of the scale propagation over multiple years is evaluated with the
38 regular analysis of target air cylinders and with long-term same air measurement comparison efforts with
39 WMO GAW partner laboratories. Long-term calibrated, globally distributed and freely accessible
40 measurements of H₂ and other gasses and isotopes continue to be essential to track and interpret regional
41 and global changes in the atmosphere composition. The adoption of the MPI X2009 H₂ calibration scale
42 and subsequent reprocessing of NOAA atmospheric data constitute a significant improvement in the
43 NOAA H₂ measurement records.



44 1 Introduction

45

46 High quality and sustained observations are essential to track and study changes in atmospheric trace gas
47 distributions. Ambient air measurement programs for trace gasses provide objective data to track air
48 pollution levels [Oltmans and Levy, 1994; Thomson et al., 2004; Tørseth et al., 2012; Schultz et al., 2015;
49 Cooper et al., 2020; WMO, 2022], to study how a mix of sources (and sinks) impact the air composition
50 [Ciais et al., 1995; Langenfelds et al., 2002; Brito et al., 2015] and to constrain and evaluate fluxes and
51 their trends [von Schneidmesser et al., 2010; Simpson et al., 2012; Propper et al., 2015; Montzka et al.,
52 2018; Friedlingstein, 2022; Heiskanen et al., 2022; Storm et al., 2023] at scales of interest.

53

54 H₂ is a trace gas in the Earth's atmosphere and its abundance can indirectly impact climate and air quality.
55 The analysis of H₂ measurements in firm air collected in Antarctica reveal that H₂ levels in the high
56 southern hemisphere grew by some 70% (330 to 550 ppb) over the 20th century [Patterson et al., 2021;
57 2023]. Greenland firm air covers less depth and time but results are consistent with a 30% increase in high
58 northern hemisphere H₂ from 1950 to the late 1980s [Patterson et al., 2023]. Growing emissions related to
59 fossil fuel burning most likely were behind this rise in H₂ [Patterson et al., 2021]. Results also show that
60 H₂ in both polar regions leveled off after the 1990s [Patterson et al., 2021, 2023].

61

62 H₂ has been viewed as a potential low or zero carbon energy carrier for close to five decades [Yap and
63 McLellan, 2023]. Since 2020 there has been renewed interest in the hydrogen economy [Yap and
64 McLellan, 2023] spurred by a rise in announcements of public and private projects to produce low carbon
65 H₂, also referred to as “blue” H₂ produced from natural gas with carbon capture, utilization and storage, or
66 “green” H₂ produced using renewable energy [Hydrogen Council and McKinsey & Company, 2023]. In
67 2021, H₂ global demand was over 94 million tonnes or 2.5 % of global final energy consumption [IEA,
68 2022]. This demand was almost entirely driven by refineries and a few industries (ammonia, methanol
69 and steel) and H₂ production almost entirely relied on fossil fuels with unabated emissions (“gray H₂”,
70 [IEA, 2022]). As of December 2023, over 1,400 announced projects globally (worth US\$ 570 billion) are
71 anticipated to increase the global H₂ production capacity by 45 million tonnes through 2030 [Hydrogen
72 Council and McKinsey & Company, 2023].

73

74 Studies of the potential short-term and long-term climate impacts of increased H₂ production and use have
75 called for more research to better understand the current and future H₂ supply chain and end-use
76 emissions of H₂ and GHGs [Ocko and Hamburg, 2022; Longden et al., 2022; de Kleijne et al., 2022;
77 Bertagni et al., 2022]. Global, high quality and sustained atmospheric measurements of H₂ can provide
78 independent information to document its distribution and study its sources and sinks and how they may
79 change.

80

81 The National Oceanic and Atmospheric Administration (NOAA) Global Cooperative Air Sampling
82 Network comprises over 50 surface and mostly remote sites (<https://gml.noaa.gov/ccgg/flask.html>). At
83 each site and on a weekly basis, local partners collect air in two 2.5-L glass flasks, and then return the
84 flasks to the NOAA Global Monitoring Laboratory (GML) in Boulder, Colorado, USA, for measurements
85 of major long-lived greenhouse gasses, carbon dioxide (CO₂), methane (CH₄), nitrous oxide (N₂O), sulfur
86 hexafluoride (SF₆), as well as carbon monoxide (CO) and hydrogen (H₂) [Conway et al., 1994; Novelli et
87 al., 1999; Dlugokencky et al., 2009]. The network is a contributor to the World Meteorological



88 Organization (WMO) Global Atmospheric Watch (GAW) Programme, which promotes and coordinates
89 international scientific efforts and free access to long-term atmospheric observations [WMO, 2022].
90
91 CO and H₂ are important trace gases that share sources with CO₂ and CH₄ (fossil fuel burning, biofuel
92 burning and wildfires). Reaction with hydroxyl radicals (OH) is the main sink for CH₄ and CO and an
93 important sink for H₂. Both H₂ and CO are also produced during the chemical oxidation of CH₄ and
94 nonmethane hydrocarbons. Soil uptake by bacteria accounts for 75% of the total H₂ sink. H₂ and CO have
95 much shorter atmospheric lifetimes than CO₂ and CH₄: 2-3 months for CO and close to 2 years for H₂.
96 The H₂ global mean atmospheric lifetime is largely driven by the soil sink strength. The H₂ lifetime
97 related to the oxidation by OH is estimated to be 8-9 years [Price et al., 2007; Warwick et al., 2022].
98
99 The “Geophysical Monitoring for Climatic Change” was the original program established by NOAA to
100 gather and analyze observations of the background atmosphere composition. GMCC started measuring
101 CO₂ in background air samples in 1968 [Komhyr et al., 1985]. CH₄ was added in 1983 [Steele et al.,
102 1987]. In the late 1980s, GMCC and its successor the Climate Monitoring and Diagnostics Laboratory
103 expanded operations to measure CO in the global network air samples to add a constraint for the study of
104 combustion sources and the global carbon budget. The analytical instrument selected consisted of a gas
105 chromatograph (GC) and a reduction gas analyzer (RGA, from Trace Analytical Inc., California) that
106 could measure both CO and H₂.
107
108 Novelli et al. [1992, 1991] first reported on testing the sampling approach (flask type, stopcock fitting,
109 wet/dry air, untaped versus taped glass flasks to minimize direct sunlight exposure) and GC-RGA
110 instrumentation for CO. Around that time, other laboratories had also adopted the GC-RGA measurement
111 technique for CO and H₂ measurements in discrete air samples or in situ. Khalil and Rasmussen [1989,
112 1990] reported on H₂ measurements of whole air samples collected weekly in triplicate electropolished
113 stainless steel flasks between October 1985 and April 1989 at the four NOAA atmospheric baseline
114 observatories (Point Barrow, Mauna Loa, Samoa, South Pole), Cape Meares, Oregon, Cape Kumukahi,
115 Hawaii and at the Cape Grim Observatory, Tasmania. These measurements showed that, contrary to CO₂,
116 CH₄, N₂O and CO, background air H₂ levels were higher in the Southern Hemisphere (SH) than in the
117 Northern Hemisphere (NH). 1985-1987 monthly mean observed H₂ ranged between 500-520 ppb at the
118 South Pole and between 455 and 520 ppb at Point Barrow. H₂ exhibited a strong seasonal cycle at
119 extratropical latitudes especially in the NH and the seasonal cycles in both hemispheres were offset by 1-2
120 months only.
121
122 In 1995, H₂ standards were prepared gravimetrically in Scott Marrin Inc. cylinders and five of them
123 (spanning 485-603 ppb) were used to define the NOAA H₂ X1996 calibration scale. Working standards
124 used between 1988 and 1996 were reassigned H₂ mole fractions and flask air measurements were
125 reprocessed to be on the X1996 scale. Novelli et al. [1999] described the early NOAA H₂ measurements
126 and reported H₂ time series starting in the late 1980s or early 1990s (depending on the site) for 50 sites in
127 the NOAA Cooperative Global Surface Air Sampling Network.
128
129 Simmonds et al. [2000] reported in-situ high-frequency GC-RGA3 measurements of H₂ at the Mace Head
130 baseline atmospheric monitoring station on the Atlantic coast of Ireland for the 1994-1998 period. They
131 found that the background air at Mace Head had lower monthly mean H₂ (470-520 ppb) than background



132 air masses measured at the Cape Grim observatory (510-530 ppb) from July to April. Some of the 40 min
133 H₂ observations showed 10s-200 ppb short-term H₂ enhancements above baseline levels. The authors
134 derived an estimate of European emissions with an inverse model of enhanced H₂ in air masses impacted
135 by upwind sources of pollution. They also observed that nighttime measurements in low wind conditions
136 reflected local depletion of H₂. The authors derived variable mean deposition velocities and found that the
137 H₂ soil sink was likely a process that occurred year-round in the area.

138

139 After 1996 and until 2008, the NOAA H₂ measurement program used successive working standards that
140 were assigned based on GC-RGA measurements against the previous standards. With hindsight, the
141 NOAA X1996 calibration scale transfer and the early NOAA H₂ measurements had several limitations
142 which are briefly described below and in more detail in the Supplementary Information section S1.

143

144 By the late 1990s, same air or collocated air sample measurement comparison between NOAA and the
145 Commonwealth Scientific and Industrial Research Organisation (CSIRO) for the Cape Grim Observatory
146 and Alert, Canada, flask air analyses showed an increasing bias for H₂ between the two laboratories
147 [Masarie et al., 2001; Francey et al., 2003]. Further laboratory tests by several WMO/GAW measurement
148 laboratories revealed the RGA detector response was non linear and required frequent calibration.
149 Additionally measurement laboratories found that the H₂ mole fraction for air standards, especially those
150 stored in high pressure aluminum cylinders, could drift at rates of a few parts per billion (ppb) to tens of
151 ppbs per year [Novelli et al., 1999; Masarie et al., 2001; Jordan and Steinberg, 2011].

152

153 To address these compounding issues, in 2008 GML tested a new analytical instrument: a gas
154 chromatograph with a pulse discharge helium ionization detector (GC-HePDD) [Wentworth et al., 1994].
155 The technique showed very good performance with a stable and linear response over the 0-2000 ppb
156 range and it was adopted for the calibration scale propagation and flask air analysis in 2009 [Novelli et
157 al., 2009]. Around that time NOAA also began testing electropolished stainless steel cylinders (Essex
158 Industries, St. Louis, MO) filled with dry air for stability.

159

160 In 2007-2008, GML prepared six new gravimetric air mixtures in electropolished stainless steel cylinders
161 spanning 250-600 ppb H₂. At that time, the new gravimetric mixtures differed by about +20 ppb
162 compared to two H₂ secondary standards values assigned on the NOAA H₂ X1996 scale. For the next
163 decade, GML kept using the X1996 calibration scale while also conducting routine measurements of the
164 H₂ secondary standards against the 2007/2008 gravimetric mixtures.

165

166 The GC-HePDD H₂ measurements on the NOAA H₂ X1996 remained biased compared to GAW partner
167 measurements and the NOAA H₂ data from the global network flasks were not released publicly. SI
168 sections S1-3 provide background information on issues impacting the 1988-2008 NOAA H₂
169 measurements on RGAs, and related information from the CSIRO and Max-Planck Institute for
170 Biogeochemistry (MPI-BGC) H₂ measurement programs. The best NOAA H₂ measurement records date
171 back to 2009/2010 and are the main focus of this paper.

172

173 In Fall 2020, GML initiated an effort to 1) adopt the MPI X2009 H₂ calibration scale [Jordan and
174 Steinberg, 2011] for future measurements and 2) convert GML H₂ measurements made on GC-HePDD
175 instruments (beginning in late 2009) to that scale. This paper describes the MPI X2009 H₂ calibration



176 scale propagation within GML and the revised measurements from the NOAA Global Cooperative Air
177 Sampling Network flask air samples analyzed since late 2009. We show very good agreement for the
178 reprocessed NOAA H₂ data for different WMO/GAW measurement comparison efforts. The revised
179 NOAA GML flask air H₂ dry air mole fraction measurement records for 70 surface sites from 2009-2021
180 are publicly available [Pétron et al., 2023a]. This new dataset complements other WMO/GAW H₂
181 measurement datasets and provides reliable observational constraints for the study of atmospheric H₂
182 global distribution and budget since 2009. Future NOAA H₂ dataset updates will be released as we use
183 continued calibration results to reliably track the drift in working standards and revise their assignments.
184

185 **2 Adoption of the MPI X2009 H₂ calibration scale**

186
187 In this section, we introduce the GML H₂ calibration standard hierarchy. First we introduce the GML H₂
188 primary standards. Then we describe the GML tank air H₂ calibration system and the scale transfer from
189 the primary standards to secondary and tertiary standards (2009-April 2019) or from the primary
190 standards to working standards (after April 2019). The tertiary standards and working standards are used
191 to calibrate the H₂ instrument response on the flask air analysis systems and value assign discrete air
192 measurements. An important quality assurance procedure within GML is the routine measurement of
193 dedicated quality control cylinders (referred to as "Target" tanks) to track instrument performance.
194 Results are discussed in relation to the uncertainty of the flask air analysis systems and consistency of the
195 MPI X2009 H₂ scale implementation.
196

197 **2.1 GML H₂ primary standards**

198
199 In 2007-2008, six air mixtures spanning a range of H₂ dry air mole fractions were prepared
200 gravimetrically in electropolished stainless steel 34L cylinders ([Novelli et al., 2009], and Table 1). The
201 highest H₂ mole fraction tank developed a leak and was lost. The remaining set of five standards covered
202 the range 250 ppb to 600 ppb for H₂. Three standards in electropolished stainless steel cylinders were
203 added in 2019 to extend the upper limit of the calibration range to 700 ppb H₂ and evaluate the stability of
204 the initial set over the intervening years. These eight standards have been designated by GML as our
205 highest level H₂ standards. We refer to them as the NOAA H₂ primary standards throughout this document
206 even though they are not defining the scale.
207

208 The eight primary standards were analyzed by the WMO Central Calibration Laboratory (CCL) for H₂
209 hosted by the MPI-BGC in Jena, Germany, on their GC-PDD system in November 2020. The results
210 listed in Table 1 are reported on the MPI X2009 H₂ calibration scale [Jordan and Steinberg, 2011]. The
211 CCL uncertainty estimates listed in Table 1 refer to the standard deviation of the 25-32 discrete H₂
212 measurements made for each standard. Until they are recalibrated by the CCL, we add an 0.5 ppb 1-sigma
213 uncertainty to these assignments. This is the currently reported CCL reproducibility for their GC-HePDD
214 H₂ measurements. It accounts for potential longer term uncertainty in calibration results that would not be
215 evident in the standard deviations of measurements made close in time.
216

217 **2.2 MPI X2009 H₂ calibration scale transfer**

218



219 GML has separate, dedicated analytical systems for scale propagation and flask air analyses. Novelli et al.
220 [2009] describe the GC-HePDD instruments and the operating parameters in detail. GML has used three
221 GC-HePDD instruments so far. Each is identified by a unique internal instrument id: H9 (Agilent 6890
222 GC, serial number US10326037) for tank calibrations and H8 (Agilent 6890 GC, serial number
223 US10326011) and H11 (Agilent 7890 GC, serial number US10834030) for flask analyses. The
224 GC-HePDD instruments' responses are linear (within 0.3%) up to 2000 ppb. They are configured for ppb
225 level sensitivity and calibrated over the 200-700 ppb range, which is optimal for global and regional
226 background air analysis.

227

228 The GML H₂ primary standards are used to periodically calibrate the H9 instrument response for the
229 analysis and value assignment of lower level standards. GML used secondary standards from 2009
230 through April 2019 in the calibration hierarchy but has since removed this level to reduce the number of
231 standards which can potentially drift (see discussion of drifting cylinders later in this document). The
232 stability and longevity of the primary standards are critical to ensure the consistency of the GML H₂
233 measurements over long periods of time as required for trend analysis.

234

235 The H₂ secondary and tertiary (or working standards) used in GML are whole air mixtures in high
236 pressure aluminum cylinders (Luxfer USA). Most were filled at the GML standard air preparation facility
237 at the Niwot Ridge mountain research station using a Rix Industries (Benicia, CA) SA6 oil-free
238 compressor [Kitzis, 2017]. Two additional tertiary standards (CB11551 and CC305198) were purchased
239 from Scott Marrin. All GML tank air mixtures have a unique combination of an alphanumeric cylinder ID
240 and a fill code letter (A-Z) tied to a fill date.

241

242 Aluminum tanks are known to be unstable for storing H₂ in air standards [Jordan and Steinberg, 2011].
243 Therefore regular analyses of working standards on the tank calibrations system are critical for
244 quantifying drift to allow a time dependent value assignment on the X2009 H₂ calibration scale.

245

246 The calibration history for a secondary, tertiary or working standard only uses retained (valid) calibration
247 event results on H9. GML uses python software developed in house to write instrument output files and to
248 calculate a calibration event result. Another piece of python code is used to analyze tank air calibration
249 histories and evaluate if the H₂ mole fraction in the tank is stable or if it changes over time. For many
250 GML H₂ calibration standards and target air tanks, a linear or quadratic function is the best fit through
251 their calibration history. When this happens, the function coefficients define the tank time-dependent
252 assignment. All mole fraction assignments for standards used to propagate a calibration scale are stored in
253 a database table that can be accessed by the data processing software. As new calibration results are
254 available, the drift correction and assignment for a particular tank ID and fill code is revised as needed
255 and the affected data is reprocessed.

256

257 **2.2.1 Tank calibration system 2009-2019 configuration**

258

259 From 2007 through mid-April 2019, the H₂ tank air calibration on the H9 instrument was conducted using
260 a single standard gas (primary or secondary standard) to calibrate the “unknown” (secondary or tertiary)
261 standards. Each calibration event consisted of alternating injections of the reference gas and the
262 “unknown” with typically seven or more unknown air injections. The first aliquot in a multi injection



263 measurement sequence on H9 is often slightly biased (due to subtle timing differences with the regulator
264 flush cycle) and is not used. The ratio of the H₂ peak height for each valid “unknown” air injection and
265 the mean peak height of two bracketing reference gas injections (or sometimes only one preceding or
266 following reference gas injection) is multiplied by the reference/standard gas known H₂ mole fraction to
267 calculate the “unknown” air injection mole fraction. Results for a tank air calibration event are defined by
268 the mean and the standard deviation of the calculated H₂ mole fractions for five or more retained
269 unknown air injections. Typically, the standard deviation for a tank air calibration event on H9 is less than
270 1 ppb.

271

272 Prior to the 2023 GML H₂ data reprocessing, GML used peak area for the GC-HePDD as described in
273 Novelli et al. [1999]. However, we saw that for some Helium carrier gas tanks (Airgas Ultra High Purity,
274 99.999% purity), the H₂ chromatogram peak had a tail or a noisy baseline. Since the H₂ peak height was
275 less affected, we use peak height ratios for all GC-HePDD measurements. In 2023, GML switched to
276 Matheson Research Grade Helium carrier gas for the GC-HePDDs (99.9999% purity).

277

278 Two secondary standards with background ambient air level H₂ were in service on H9 to calibrate tertiary
279 standards: CC119811 (2008/02 to 2013/06) and CA03233 (2013/06 to 2018/11). These two standards
280 were calibrated periodically on H9 against individual members of the primary standard suite. Most
281 calibration episodes consisted of one to 6 calibration sequences over 1-3 successive days, each against
282 one of the primary standards. For CC119811, 1-point calibration sequence results in 2008, 2009, 2010 and
283 2013 against one of the two lowest primary standards (SX-3558 and SX-3543) show a 3 to 5 ppb positive
284 bias which suggests a small non zero intercept in the instrument response during those times. This
285 primary standard dependent bias is not apparent for CA03233 results between 2014 and 2016. Results
286 against SX-3558 were not used for value assigning either secondary standards and results against
287 SX-3543 were not used for CC119811.

288

289 The calibration results for the two H₂ secondary standards are plotted in Figure 1 and final assignments
290 are listed in Table 2. CA03233 was stable for H₂ over its time of use and has an assignment of 502.8 ppb
291 H₂. H₂ in CC119811 exhibited a small linear drift and its value assignment is time dependent with a
292 growth rate of 2 ppb/yr. Between 2009 and 2019, the two secondary standards were used on H9 to
293 calibrate seventeen H₂ tertiary standards used in the NOAA discrete air sample analysis laboratory.

294

295 2.2.2 Tank air calibration system 2019-present configuration

296

297 Beginning in April 2019, GML transitioned H9 to use a multi-point calibration strategy to better define
298 the instrument response. The eight H₂ primary standards are measured relative to a reference air tank
299 (CC49559, filled at ambient Niwot Ridge air) to calibrate the instrument response. A multi-standard
300 response calibration episode for H9 involves the alternating injections from the reference air tank and
301 each primary standard. Each standard is injected 8 times alternating with reference air aliquots. The entire
302 response calibration sequence takes close to 15 hours. GML has performed an H9 instrument response
303 calibration followed by tank calibrations a few times a year over a 10-14 day period each time.

304

305 The H9 instrument response function is calculated as the best linear fit to the primary standards’ mean
306 normalized chromatogram peak heights and their CCL H₂ mole fraction assignments. H9 calibration



307 curves are assumed to be valid for several weeks during which time other air cylinders are analyzed
308 relative to the same reference tank.

309

310 Between April 2019 and December 2022, H9 instrument response was calibrated nine times. Figure 2a
311 shows the deviations of the H9 linear response functions from the line defined by computing the mean
312 value for the intercept and slope of the 2019-2022 response functions. The instrument response has
313 remained stable within +/- 1 ppb over this time period over the range 200-700 ppb. Figure 2b shows the
314 residuals to the best linear fit for each instrument response calibration episode. We note that the H9
315 instrument response has been quite stable over the 200-700 ppb range but that the linear fit does not go
316 through the origin. The residuals to the linear fit over this time period are all within the -0.6 ppb to 0.5
317 ppb range. The linear fit y-intercept ranges between 3.9 and 5.5 ppb (not shown). Prior to 2019, we
318 assumed a zero intercept for the H9 one point calibration. If we assume a y-intercept around 5 ppb was
319 more likely, it is possible the pre-2019 H9 measurements (with 1 point calibration) were biased by ~1% of
320 the difference between the tank air and the standard H₂ mole fractions. We do not correct for this potential
321 bias at this time.

322

323 A tank air measurement sequence typically consists of 7 injections, each bracketed by reference air
324 injections. The peak heights for the first injections of reference air and tank air on H9 can have a small
325 low bias and are not used. The normalized peak heights for the valid tank air injections are converted to
326 H₂ mole fractions using the most recent H9 instrument response calibration episode. The average and
327 standard deviation of the retained injection H₂ mole fractions are stored in a database table.

328

329 **2.2.3 H₂ standards and calibration approach for the flask air analysis system**

330

331 The NOAA Global Cooperative Air Sampling Network dates back to 1967. In recent years, it has
332 included over 50 surface sites distributed around the world
333 (https://gml.noaa.gov/ccgg/behind_the_scenes/network.html). Partners at each site collect air sample pairs
334 in two 2.5L glass flasks filled simultaneously once a week and return the samples to NOAA GML in
335 Boulder. H₂ in those flask air samples is measured in addition to long-lived GHGs (CO₂, CH₄, N₂O, SF₆)
336 and CO by the Measurement of Atmospheric Gases that Influence Climate Change (MAGICC) system in
337 the NOAA GML Boulder laboratory. Until mid 2019, GML operated two nearly-identical automated flask
338 air analytical systems: MAGICC-1 (1997-2019) and MAGICC-2 (2003-2014). Since mid-2019, GML has
339 used a new MAGICC-3 system. This new system improved analytical techniques for CO₂, CH₄, N₂O, and
340 CO but continues to use the same GC-HePDD instruments from the older systems.

341

342 Two GC-HePDD instruments have been used for hydrogen analysis on the three flask air analysis systems
343 since 2009: H8 (MAGICC-2: 2009-2014 and MAGICC-3: August 2019-September 2020) and H11
344 (MAGICC-1: 2010-July 2019 and MAGICC-3: September 2020-present).

345 On MAGICC-1 and MAGICC-2, the He-PDD instrument response was calibrated using a single tertiary
346 standard (measured before and after each sample aliquot), similar to the original approach used on H9.

347 Typically, the H₂ tertiary standards used during that time lasted less than a year and most displayed H₂
348 growth over time. Figure 3 shows the calibration histories for H8 and H11 tertiary standards and their
349 start/deployment dates. Table 2 provides a list of the standard cylinder IDs and fill codes and information



350 for their mole fraction assignments: t_0 date, the best polynomial function fit coefficients relative to time t_0
351 ($c_i, i=0,2$) and an estimated 1-sigma uncertainty. The uncertainty is empirically derived and based on the
352 standard calibration history and the standard deviation of the residuals to the best fit (the assignment). The
353 python code used to calculate the tertiary standard assignment uses a 0.5 ppb 1-sigma reproducibility
354 uncertainty which is added in quadrature to the measurement episode standard deviation to account for
355 longer term uncertainties not evident in the standard deviation of the n-aliquots. We do not formally
356 include an uncertainty for the secondary standard assignment. The H9 reproducibility term is based on the
357 mean of the standard deviation of residuals to the fit for the calibration histories of secondary standards
358 and target tanks over the period 2008-2022 (see section 2.3.1).

359 The number of tertiary standards used successively on the older systems introduces time dependent issues
360 due to the variable rate of H_2 drift in aluminum tanks and the frequency of the tank calibrations on the
361 calibration system. Some of the H11 tertiary standards only have pre-deployment calibration results which
362 do not assess drift during use (CC71649, CA04505, CC105491) and other standards have calibration
363 results during their time in use but do not have post deployment calibrations that may help us evaluate the
364 drift rate for the last couple of weeks or months of use (ND46735, ND33801, CB11551, CB11090,
365 CA08107). A few standards exhibited an increased drift rate towards the end of their life that we did not
366 capture with the infrequent calibrations on H9. This change in drift behavior was observed as increasing
367 biases for measurements of target air tanks and daily test air flasks (see section 3.2). We have applied
368 offline mole fraction corrections to the flask air analysis H_2 results to correct for the end of use drift
369 increase for tertiary standards CC71649 (H11), CB11551 (H11) and CC305198 (H8), and the standards'
370 assignment uncertainty is larger for these time periods (Table 2).

371 Since August 2019, GML has used a newer analytical system (called MAGICC-3) in the flask air analysis
372 laboratory with a GC-HePDD (instrument code H8 and later H11) for H_2 , new optical analyzers for CO_2 ,
373 CH_4 (CRDS, Picarro), CO and N_2O (QC-TILDAS, Aerodyne), and a GC-ECD for SF_6 . The responses of
374 the instruments on MAGICC-3 are calibrated at the same time using a single set of 11 standards spanning
375 a range of mole fractions for the six trace gasses. The MAGICC-3 standards were filled at the Niwot
376 Ridge standard air preparation facility. They are regularly measured on H9 against the GML H_2 primary
377 standards.

378 For the MAGICC-3 instrument response calibration, the eleven standards are analyzed sequentially
379 relative to an uncalibrated reference air tank (filled at Niwot Ridge). Air from each standard is injected 6
380 times alternating with the reference air. This entire sequence takes close to 17 hours. The first injection of
381 each standard is often biased low by about 2 ppb for H_2 due to timing issues at the start of each standard
382 sequence and only the remaining 5 injections are used to obtain the average normalized peak height
383 "signal" for each standard.

384 For H_2 , a subset of 8 of the 11 working standards are used to calibrate the GC-HePDD response. The
385 time-dependent H_2 value assignment for each standard was derived from 8 or 9 calibration events on H9
386 between June 2018 and December 2022, listed in Table 3 (Table 3, SI Figures 1 and 2). We plan on
387 analyzing the MAGICC-3 standards 2 to 3 times a year going forward. The standards' H_2 assignments will
388 be revised as needed.

389 The time between calibration sequences was 2 weeks for the first 3 months of service of MAGICC-3 and



390 it has been increased to 4-5 weeks as we found the results to be quite stable. A reference air cylinder will
391 last 9 to 12 months on MAGICC-3. When the MAGICC-3 reference air cylinder is changed (pressure
392 close 250 psia), a new instrument calibration episode is done with the new reference air cylinder before
393 flask air samples are analyzed.

394 For the asynchronous calibration to stay valid up to 5 weeks requires the reference gas composition for
395 the six measured gasses to be stable between successive calibration dates. This has been true so far except
396 for one reference air cylinder CA04145 for which a small time dependent H₂ correction was applied
397 between instrument response calibration dates from 2019-11-06 to 2020-01-16 (see SI Figure 3 and more
398 details in SI section S4).

399 **2.3 Calibration scale transfer quality assurance**

400

401 GML target air tanks are dedicated air mixtures used for measurement quality control over multi-year
402 periods. Most are high pressure aluminum cylinders filled at the Niwot Ridge standard preparation
403 facility. The analysis of target air helps us evaluate the robustness of the calibration scale transfer, and the
404 consistency of measurements over time and also between different analytical systems. In a perfect
405 program, we should be able to reproduce a measurement result for a target air tank every time. As noted
406 earlier, however, the reality is more complicated as H₂ tends to grow with time in aluminum cylinders.
407 Tracking many aluminum cylinders provides a diverse history of behaviors (stable, or linear vs non-linear
408 drift), and aids in the understanding of similar cylinders used for calibration.

409

410 **2.3.1 Calibration system (H9) Target air tanks**

411

412 Some GML target air cylinders are used exclusively to evaluate the stability and performance of the H9
413 measurements. Other target air cylinders are analyzed on H9 and in the flask air analysis laboratory on the
414 H8 and H11 instruments to understand the scale transfer.

415

416 While H₂ has been increasing in most of our target air tanks, eleven H9 target air tanks have shown either
417 stable H₂ or a linear rate of increase less than 1 ppb/yr. Figure 4 shows the calibration histories for these
418 tanks as well as the residuals from the best fit for each tank. Table 4 has a list of these target tanks and
419 several others binned by linear drift rate. More details for target tanks and their trend best fit coefficients
420 are in SI Table S1. For each bin, the standard deviation of the residuals (differences of the H9 calibration
421 results minus the best fit values) is below 0.5 ppb. The standard deviation of all linearly drifting target
422 tanks residuals binned together is 0.4 ppb.

423

424 The regular analysis of target tanks on H9 (right after the instrument response has been calibrated against
425 the primary standards) is used to evaluate the robustness of the calibration scale transfer in GML. Results
426 for tanks with stable or very slowly drifting H₂ indicate that between 2008 and 2021, the scale transfer on
427 H9 has low uncertainty (< 1 ppb).

428

429 We have eleven other target tanks for which the best fit to their calibration history is a quadratic function
430 (SI Figure 4 and SI Table S1). The standard deviation of these tanks' residuals binned together is 0.7 ppb.
431 The current set of H9 target air tank results show that residuals for higher mole fraction (>650 ppb) tanks
432 have a larger standard deviation (0.5-0.8 ppb, SI Figure 4d).



433

434 One tank (CC309852 A, fill date 2009-10-01) with a quadratic drift correction is on the lower end of the
435 GML calibration range with a H₂ mole fraction that grew from 204 ppb in 2009 to 232 ppb in 2021. The
436 standard deviation for this target tank residuals is 0.93 ppb. It appears that a quadratic fit does not capture
437 the observed growth very well. If we reject the first calibration result in 2009 and only fit the other
438 2011-2021 results showing the H₂ mole fraction increasing from 217 ppb to 232 ppb, the best fit is a still a
439 quadratic function but with smaller coefficients ($c_1 = 1.66$ ppb and $c_2 = -0.16$ ppb) and the standard
440 deviation of the residuals to this fit is reduced to 0.36 ppb. Similarly, other tanks that were analyzed soon
441 after fill and over several years show a similar rapid and large initial growth in H₂ (in the first 0.5-2 years
442 after fill). In this scenario, the residuals to a best linear or quadratic fit of the full calibration history will
443 be larger and will likely not capture the tank time-dependent H₂ assignment as accurately. For a few of the
444 GML standard and target air tanks, we dropped early calibration results that would bias the best fit
445 derivation and assignment during the time of use of the tank.

446

447 2.3.2 Comparison of measurements of gas mixtures in cylinders with MPI-BGC

448

449 Since 2016, the MPI-BGC GasLab has organized same tank air measurement (“MENI”) comparisons
450 between WMO GAW partner laboratories as part of the European ICOS (Integrated Carbon Observation
451 System) Flask and Calibration Laboratory quality control work. In this program, three high pressure
452 cylinders are prepared and maintained by the MPI-BGC and sent to measurement laboratories in a round
453 robin loop. Two of the three cylinders had the same air mixture and showed small growth in their H₂ mole
454 fractions over time. The third cylinder contains an “unknown” new mixture for each round robin loop.

455

456 Between 2016 and 2021, the MENI cylinders came to GML three times and were analyzed two to four
457 times on the H9 instrument during each round robin stop (see SI Figure 5). Some results were rejected
458 due to poor instrument performance or the use of an alternate calibration strategy than the one used to
459 transfer the scale. For the ambient and blind H₂ MENI cylinders the retained NOAA H₂ results agree well
460 with the MPI_BGC measurements (< 1 ppb difference). For the low H₂ cylinder, the 2017/2018 NOAA
461 measurements are biased low by about 2 ppb while the March 10, 2021 result is about 2 ppb higher (SI
462 Figure 5c). The MENI program provides an important on-going check for the MPI X2009 H₂ calibration
463 scale transfer in GML.

464

465 2.3.3 Flask analysis system (H8, H11) target air tanks

466

467 Figure 5 shows the calibration histories for target air tanks used in the flask analysis laboratory between
468 2009 and 2022. H₂ increased in all the target tanks, sometimes rapidly, requiring time dependent value
469 assignments. These time-dependent H₂ assignments are derived from the best linear or quadratic fit to the
470 calibration results on H9. These assignments can be compared to the measurements on the flask analysis
471 systems to evaluate the quality of the scale transfer. It should be noted that the non-linear drift of some of
472 these tanks may not be well modeled by a simple quadratic function, leading to higher uncertainty in the
473 value assignments. This is especially true for tanks with limited calibration histories or gaps in their
474 calibration histories.

475



476 Three H₂ target air tanks were in service between 2009 and 2019 and have been used to evaluate the GML
477 calibration scale transfer to the MAGICC-1 and MAGICC-2 H₂ measurements (CC1824 (H), CB08834
478 (B) and CC303036 (A)). These tanks, however, exhibited rapid and large drifts and were not measured on
479 H9 on a regular basis making it more difficult to use them to evaluate potential biases on MAGICC-1 and
480 MAGICC-2 over this time period.

481

482 The target air tanks ALMX067998 (C) and CB11143 (C) entered service in 2016 and 2019 respectively
483 with more frequent measurements on the calibration system to better define the time dependent value
484 assignments. A new set of six target air tanks were prepared at the Niwot Ridge facility in late 2019 for
485 the MAGICC-3 system. They have been analyzed on MAGICC-3 multiple times a year but only one of
486 them has a H₂ mole fraction that remained below 700 ppb: CB10292 (B).

487

488 With the caveats that the non-linear drift in aluminum cylinders may not be well modeled by a simple
489 quadratic polynomial and that many of the early target tanks were under calibrated, the best polynomial fit
490 to the calibration records for all target air tanks give residuals smaller than 1.2 ppb. Details for the target
491 tanks, including the best fit coefficients and the standard deviation of residuals to the fits are in SI Table
492 S2. The uncertainty on the assignments is larger during extended time periods with no calibration results
493 especially for the 3 earlier target air tanks with a limited calibration history (CC1824 (H)) or with
494 calibration histories showing evidence of a change in the drift rate (CB08834 (B) and CC303036 (A), see
495 Figure 5).

496

497 In Figure 6, we show the differences between the target air analysis results on H8 and H11 and their
498 time-dependent H₂ assignments (based on the best fit to their calibration histories on H9 discussed above).
499 The differences are all within 4 ppb, however there are clearly times when there are persistent biases
500 between the flask analysis system(s) and the calibration system. Uncertainties on the value assignment of
501 the target air tanks, the value assignments and stability of the standards used to calibrate the flask analysis
502 systems as well as the noise in the H8 and H11 measurements all contribute to the observed differences.
503 Similar offsets on both flask analysis systems (for example CC1824 prior to 2012) may point to the main
504 uncertainty contribution being from the value assignment of the target air tank. Different patterns in the
505 offsets between the two flask analysis systems (for example offsets of different signs for CC303036 (A)
506 and CB08834 (B) on H8 and H11 in 2011-2013) suggest the offsets are due to value assignments of the
507 flask analysis system standards. Again, this is often due to limited calibration histories not being able to
508 fully map the non-linear drift in the standards. It also indicates there are times with systematic differences
509 (mostly < 2ppb) between the MAGICC-1/H11 and MAGICC-2/H8 measurements in the flask records.

510

511 The full transition to the new MAGICC-3 system for flask analyses in August 2019 is indicated by the
512 vertical bar in Figure 6. As discussed earlier, one improvement in this new system is that H₂
513 measurements are now calibrated using a multi-point calibration curve from a suite of standards. This
514 makes the measurement results less sensitive to drift or value assignment error in any individual standard
515 since we are fitting multiple standards. These standards are used once a month and thus have much longer
516 lifetimes and longer calibration histories. We also now appreciate the complex H₂ growth patterns that can
517 occur in aluminum cylinders so have undertaken regular calibrations to ensure drift is tracked closely.
518 These changes seem to have reduced the bias observed between the flask analysis system and the
519 calibration system, which gives confidence that future measurements will be higher quality.



520

521 To help us monitor the H₂ calibration scale propagation going forward, a new target air tank in an Essex
522 stainless steel cylinder, SX-1009237, was filled in late 2022 to augment the current target tanks. This
523 target air tank should be stable for H₂ and will be used for periodic comparison between measurement
524 systems. Analysis results on H9 and H11 in December 2022 are 526.75 and 527.15 ppb, respectively,
525 consistent with the residuals for other target air tanks at that time.

526

527 **3 NOAA flask air H₂ measurements**

528

529 Close to 6000 flask air samples from the Global Cooperative Air Sampling Network are analyzed in GML
530 every year. The network sites are chosen carefully to be representative of large scale air masses and to be
531 able to rely on local support for sampling and shipping logistics. The reprocessing and release of the
532 2009-2021 H₂ global network flask air measurements on the MPI X2009 scale was made possible because
533 of continued efforts to conduct and improve the H₂ measurements, to store all the necessary data, and to
534 develop and update the tools for reliable and traceable reprocessing, comparison, and archiving.

535

536 **3.1 Recapitulation of the GML flask air H₂ analysis system configurations since 2009**

537

538 The MAGICC-2 H8 and MAGICC-1 H11 instruments started routine flask air H₂ analyses on November
539 5, 2009 and February 9, 2010 respectively. The flask air analysis results have been reprocessed using the
540 tertiary standards or working standards time-dependent H₂ assignments on the MPI X2009 scale. As
541 mentioned earlier, those flask air measurements on H8 and H11 until July 2019 relied on calibration with
542 a single tertiary standard also used as reference to normalize the air sample chromatogram H₂ peak height.

543

544 After August 2019, the MAGICC-3 system uses a multi-standard instrument response calibration. For H₂,
545 the instrument response curve is derived from eight working standards “known” assignments and their
546 normalized H₂ peak heights, with a reference air that is not a standard. H8 was the H₂ instrument on
547 MAGICC-3 until September 11, 2020 when it was replaced by H11 which has better precision. The linear
548 fit coefficients for the MAGICC-3 H8 and H11 response curves are stored and used to calculate the H₂ dry
549 air mole fraction in unknown air samples.

550

551 **3.2 Data quality assurance and quality control**

552

553 GML flask air H₂ measurements data quality is evaluated using results from the daily analysis of test air
554 flask pairs and from the agreement between South Pole Observatory flasks pairs.

555

556 In this section, we first describe the flask sample collection protocol and introduce the data quality control
557 tags used to document sample and measurement data quality issues. Then we assess the GML H₂
558 measurement short-term repeatability with statistics from test air flasks and South Pole Observatory flask
559 pair differences. Finally, we present a preliminary estimation for the uncertainty of flask air H₂
560 measurements over 2009-2021, that includes empirical uncertainty estimates for the standards’
561 assignments and the short-term noise of the instruments.

562

563 **3.2.1 Flask air sample collection overview and data quality tagging**



564

565 Partners in the NOAA Global Cooperative Air Sampling Network collect whole outside air samples in
566 glass flasks in pairs, upwind from any local sources of pollution, people and animals and away from
567 structures or terrain that would affect the wind flow. Two 2.5L glass flasks with two glass stopcocks with
568 Teflon o-rings are connected in series in a portable sampling unit (PSU) made of a rugged case, a battery,
569 a pump, an intake line, and a mechanism to control the pressure of the air samples. Most sampling units
570 include a dryer and are semi-automated, with the exception of those used at relatively dry high latitude
571 locations and a few other locations where a more rugged, manually operated sampling unit is required. At
572 most sites, the operator will carry the equipment outdoors to conduct the sampling. At a few sites, the
573 PSU is indoors and connected to a fixed inlet line drawing air from the outside.

574

575 Before shipment, the glass flasks are filled with synthetic air in the GML flask logistics laboratory.
576 During the sample collection on site, the flasks are first flushed for several minutes and then filled to a
577 pressure of 4 to 5 psi above ambient pressure in about 1 minute (See video:
578 <https://gml.noaa.gov/education/intheair.html>).

579

580 Air sample collection and/or measurement issues that are documented or detected and known to affect a
581 sample quality or an analyte measurement result are recorded with data quality control tags in our internal
582 database. For each flask air measurement, internal data quality control tags are translated into a simpler 3
583 column flag indicating if the measurement is retained or rejected for external data users. The GML flask
584 air samples and measurements can also have informational tags and comments, for example if another
585 measurement laboratory analyzed an air sample before it came to GML for analysis (see same air flask
586 comparisons in section 3.3).

587

588 The global network flasks are filled to target pressure of 17-20 psia, but the final fill pressure can vary by
589 a few psi, with some of the higher altitude sites having final pressures on the lower range typically. If an
590 air sample pressure is too low for the H₂ GC instrument on the MAGICC system, the H₂ measurement
591 result is tagged as “rejected” for low sample pressure. If H₂ measurements in paired flasks have a 5 ppb or
592 larger difference, the results for the pair are tagged as rejected. If only one member of the pair had an
593 obvious issue (leak, low flask air pressure), only the H₂ measurement for that member is tagged as
594 rejected. Some issues are detected by the MAGICC performance control system and are tagged
595 automatically. Other issues are tagged manually by scientists as part of regular data quality control
596 checks. Scientists also verify the validity of the automatic tags. Members of the team routinely evaluate if
597 follow-up actions are needed to fix an issue or reduce the chance of rejecting future samples for the same
598 issue.

599

600 Some sites can experience brief high-pollution episodes with measurements in both members of a pair
601 meeting the pair agreement criteria but also being outliers, i.e. outside of the expected long-term
602 variability at the site. For each site, we applied a smoothing curve fit calculation to determine the time
603 series mean behavior broken down in a long-term trend, a seasonal cycle, and shorter-term (hours to
604 weeks) variations [Thoning et al., 1989; Tans et al., 1989a]. The code is available and a link is provided
605 further down. Measurements that show large residuals from the fit are not representative of the typical
606 background air composition at the site and are tagged as outliers [Novelli et al., 1999]. Gross H₂ outliers
607 are typically “tagged” manually. We also apply a statistical filter before each data release, which works



608 iteratively to find and tag outlier H_2 measurements when their residuals to the curve fit is larger than 3 to
609 4 times the time series residuals' standard deviation.

610

611 3.2.2 Test air flask analysis results

612

613 Besides the regular analysis of target cylinders, the MAGICC flask analysis system is also routinely tested
614 using flasks filled with “test air” (flasks with site code “TST”). TST flasks are filled in one batch with air
615 from one of four high pressure aluminum cylinders (AL47-104, AL47-108, AL47-113, AL47-145),
616 themselves filled at the Niwot Ridge standard preparation site. SI Figure 6 shows the calibration histories
617 on H9 for different fills for these four test air cylinders. H_2 is not stable in the “test air” cylinders and for
618 some tank-fills, H_2 increased rapidly and grew beyond our calibration range upper limit of 700 ppb.

619

620 Every 2 to 3 weeks, the GML flask preparation and logistics laboratory manager fills an even number of
621 TST flasks (14-24) from the same test air cylinder. On typical analysis days, the MAGICC flask air
622 measurement sequence will start with the analysis of air from two TST flasks with the same fill date.
623 Global network flask air samples are analyzed at NOAA GML only during the daytime to ensure the
624 system operator is overseeing the full analysis cycle and minimizing the time a flask valve is open for the
625 analysis. This is meant to minimize the risk of losing or contaminating the air samples as many of them
626 are subsequently sent to the University of Colorado Boulder Stable Isotopes Laboratory for CO_2 and CH_4
627 isotope analyses.

628

629 Results from the TST flask pairs with the same fill date and analyzed on successive days give an
630 indication of the short-term repeatability of the measurements. Here, the deviations from the mean H_2 in
631 TST flasks with the same fill date are evaluated. For fill dates with a mean H_2 mole fraction less than 700
632 ppb, we calculate the differences between individual TST flask H_2 and the fill date mean. The standard
633 deviation of the TST flasks H_2 differences from their fill date mean is 1.39 ppb on MAGICC-2/H8
634 (N=872), 0.73 ppb on MAGICC-1/H11 (N=3583), 1.55 ppb on MAGICC-3/H8 (N=504) and 0.68 ppb on
635 MAGICC-3/H11 (N=1085), reflecting the higher measurement noise on H8.

636

637 Another diagnostic is the comparison of the TST flasks H_2 results and their test air cylinders'
638 time-dependent assignments for the dates the TST flasks were filled based on the best fit of the H9 test air
639 tank calibration results. This analysis is limited to the test air cylinders and fill code(s) with less than 700
640 ppb H_2 and with tank calibration results on H9 that reasonably capture the increase in H_2 : AL47-108 (F),
641 AL47-113 (D,E,G), AL47-145 (F,G), AL47-104 (I). In SI Figure 7 (a-c), we show the H_2 differences
642 between the TST flask results and their test air cylinder assignments. The differences reflect noise in the
643 flask air measurements and uncertainties (and potentially small biases) in the test air tank-fill assigned H_2 .

644

645 The three fills of test air cylinder AL47-113 are in the ambient range and have the most stable H_2 mole
646 fractions. The tank-fill assigned H_2 linear drift rate is 1 ppb/yr in fill D, null in fill E and 0.4 ppb/yr in fill
647 G. Table 5 shows the mean and standard deviation of the differences in H_2 between TST flasks and the
648 assigned H_2 in a stable or slowly drifting test air tank-fill. The biases for these subsets of TST air data are
649 less than 1 ppb and the standard deviation is equal or less than 1.5 ppb and is smaller for the most recent
650 MAGICC-3/H11 configuration which has a smaller number of data points.

651



652 3.2.3 South Pole Observatory: H₂ differences in flask pairs

653

654 NOAA GML operates four staffed atmospheric baseline observatories (<https://gml.noaa.gov/obop/>). The
655 South Pole Observatory (SPO) in Antarctica and the Mauna Loa (MLO, Hawaii) observatories were built
656 in connection with the 1957-1958 International Geophysical Year, a global effort bringing together 67
657 nations to study the Earth and in connection with the first launches of artificial satellites in Earth's orbit
658 by the USA and the Soviet Union. The South Pole Observatory in Antarctica was established with support
659 from the US National Science Foundation and NOAA. The other two observatories near Utqiagvik,
660 formerly Barrow, (BRW) and Samoa (SMO) were established in 1973 and 1974 respectively. H₂ time
661 series for the observatories are shown in section 4.

662

663 The South Pole Observatory (site code SPO, sampling location: 89.98°S, 24.80°W, 2815 meters above sea
664 level (masl)) gives scientists access to some of the “cleanest” air on Earth due to its remote location. On
665 site, GML and partners operate in-situ measurements to monitor the atmosphere composition and
666 properties, and whole air samples have been collected for trace gas analyses in the GML laboratories in
667 Boulder since 1975.

668

669 All four NOAA atmospheric baseline observatories have an upwind clean air sector with no local sources
670 of pollution (<https://gml.noaa.gov/obop/>). Every week, scientists on location collect discrete air samples
671 when the near surface wind comes from the clean air sector. Two flask pairs are typically collected
672 weekly and close in time at the four NOAA atmospheric baseline observatories using two collection
673 methods. In method ‘S’ flasks are filled inside a building by tapping the air continuously pumped for
674 analysis on an in-situ GHG measurement system. Method, ‘P’ (or ‘G’) involves using a portable sampling
675 unit with an inlet mast and pump set up outside the building, similarly to other global network sites. The
676 scientist doing the air sampling is involved with both sampling techniques. Weekly samples with both
677 methods are typically conducted within minutes of each other. Both flask sampling methods give reliable
678 results for H₂ at the South Pole Observatory.

679

680 Staff rotation and flask shipping to and from the South Pole Observatory happen during a limited time
681 window during the Austral summer. While awaiting shipment, SPO flask air samples are stored in crates
682 in a heated storage building. Every year, one large SPO flask shipment arrives in Boulder in
683 December/January and another smaller shipment arrives in March. A year's worth of flasks is prepared
684 and shipped to SPO during that same time window. Despite the longer storage for SPO flasks before
685 analysis, we have not detected biases in H₂ measurements of those samples when compared with other
686 high southern latitudes times series. SPO flask air H₂ measurements show close to a 20 ppb seasonal cycle
687 and a ~15 ppb increase in the annual mean levels between 2010 and 2021 (Figure 7).

688

689 There is very little short-term variability in the surface air over Antarctica for long-lived GHGs, CO and
690 H₂. The differences in the H₂ mole fractions in SPO paired samples therefore mostly reflect the short-term
691 noise in the measurements. In Table 6 we report statistics for H₂ differences for the two flask sampling
692 methods and the four measurement system configurations between 2009 and 2021 with H8 and H11. As
693 observed for the TST flasks, measurements on H11 are less noisy than on H8, especially on the
694 MAGICC-3 system.

695



696 3.2.4 Flask air H₂ uncertainty estimates

697

698 We have derived preliminary empirical uncertainty estimates for flask air H₂ measurements that fall in the
699 200-700 ppb range. For measurements on MAGICC-1 and MAGICC-2, the total uncertainty estimate
700 comes from the combination of two uncertainties added in quadrature: 1) the uncertainty on the H₂ tertiary
701 standard time-dependent assignment (Table 2) and 2) the instrument estimated repeatability (Table 8). If
702 an offline assignment correction is applied to take into account changes in a standard drift rate toward the
703 end of its use, the standard assignment uncertainty is increased. The H8 and H11 instrument repeatability
704 estimates are listed in Table 8. For now, we assume a 0.5 ppb uncertainty on the MAGICC-3 instrument
705 response calibrated with multiple standards. On-going work will allow us to refine this last uncertainty
706 component estimate at a later date. Typical 1-sigma uncertainties for GML flask air H₂ measurements are
707 1.2 to 1.9 ppb on MAGICC-1, 1.4 to 2.8 ppb on MAGICC-2, 1.6 ppb on MAGICC-3/H8 and 0.8 ppb on
708 MAGICC-3/H11.

709 3.3 Comparison with other GAW laboratories H₂ measurements

710

711 A small number of laboratories operate well-calibrated long-term measurements of important atmospheric
712 trace gasses. The WMO Global Atmospheric Watch (GAW) coordinates regular technical and scientific
713 discussions with experts from these laboratories. Another important outcome of the WMO/GAW
714 collaborations consists of routine comparisons to assess the data compatibility for measurements coming
715 from different laboratories and programs [Francey et al., 1999; Masarie et al., 2001; Jordan and Steinberg,
716 2011; Worthy et al., 2023]. The WMO/GAW network compatibility goals for measurements of H₂ in well
717 mixed background air is 2 ppb (see Table 1 in [WMO/GAW, 2020]). This means that for H₂ measurement
718 records should have persistent biases less than 2 ppb to be used in combination with other qualifying
719 measurements in global budget, trend and large scale gradient analyses.

720

721 GML participates in several WMO GAW measurement comparison efforts. Same-flask air measurement
722 comparisons consist of one member of a NOAA flask pair collected at a site being analyzed by a partner
723 laboratory before being analyzed by GML. Co-located flask air measurement comparisons involve 2 or
724 more measurement programs having samples collected at the same location and close in time.
725 Historically, these and other “intercomparison” projects have been abbreviated ICPs, which we use in the
726 text below. Here the GML flask air H₂ measurements data compatibility is assessed with results from
727 on-going ICPs.

728

729 GML conducts same-flask air measurement comparisons at the Cape Grim Observatory (CGO, 40.68° S,
730 144.69° W, 164 masl) with CSIRO, Australia and at the Ochsenkopf mountain top tower (OXK, 50.03° N,
731 11.81° E, 1085 masl) with MPI/BGC, Germany. Sampling at OXK was temporarily suspended between
732 June 2019 and April 2021. The Alert/Dr Neil Trivett Observatory (ALT, 82.45° N -62.51° W, 190 masl)
733 has facilitated the largest multi-laboratory flask air comparison experiment in the WMO GAW program
734 [Worthy et al., 2023]. NOAA has collocated flask air samples from ALT with CSIRO and the MPI/BGC.
735 The CSIRO and MPI/BGC H₂ measurements are also traceable to the MPI X2009 calibration scale.

736

737 In Table 7, we summarize the annual mean of the differences for H₂ measurements from different
738 laboratory and flask combinations (same flask, same flask pair or collocated flasks) for CGO, OXK and



739 ALT between 2010 and 2021. Columns 2 and 3 show the annual means of the NOAA H₂ differences
740 between the ICP flask and its pair mate at CGO and OXK. All measurements included in the comparisons
741 are retained, meaning they have passed quality control checks.

742

743 For CGO flask air samples collected before 2019, we find that the NOAA analysis for the NOAA ICP
744 flask first measured at CSIRO often shows higher H₂ than in the non-ICP flask air sample. We suspect
745 several of these ICP flasks had a small but detectable contamination for H₂. We have applied a rejection
746 tag to NOAA analysis results for CGO ICP flasks with an H₂ mole fraction 2 ppb or more above H₂ in the
747 non-ICP pair mate. This affected 165 ICP samples between 2009 and 2018 or 37% of all CGO ICP flasks
748 collected between August 2009 and the end of 2021.

749

750 For OXK, the NOAA analysis result for the ICP flask first measured at MPI/BGC often shows slightly
751 higher H₂ than in the non-ICP flask (Table 7, 3rd column), and the annual mean bias is less than 1 ppb for
752 all years.

753

754 The last 4 columns in Table 7 show interlaboratory H₂ measurement comparisons for CGO, OXK and
755 ALT flask air samples. The annual mean differences are consistently less than 1.6 ppb for CGO (CSIRO
756 ICP flask and NOAA non ICP flask) and less than 2 ppb for OXK for 9 out of 11 years (MPI/BGC ICP
757 flask and NOAA ICP flask) (Figure 8). For colocated air samples at ALT (NOAA vs CSIRO and NOAA
758 vs MPI/BGC) we compare the mean of flask results for each laboratory and limit the comparison for
759 samples collected within 60 minutes of each other. The ALT annual mean differences vary from year to
760 year, are less than +/- 2 ppb for 8 years out of 12 for the NOAA vs CSIRO comparison and for 7 years out
761 of 10 for the NOAA vs MPI/BGC comparison. These on-going ICPs are monitored regularly to
762 continually assess the NOAA H₂ data compatibility with data from GAW partners.

763

764 4. NOAA H₂ atmospheric time series

765 Previous measurement studies have described key features of the H₂ global distribution for different time
766 periods [Khalil and Rasmussen, 1990; Novelli et al., 1999; Langenfelds et al., 2002; Price et al., 2007;
767 Yver et al., 2011]. Some of the spatiotemporal features in the more recent NOAA H₂ measurements at
768 background sites are described in this section.

769 4.1 H₂ at NOAA Baseline Atmospheric Observatories

770 Figure 9 shows the reprocessed H₂ time series for the four NOAA Baseline Atmospheric Observatories
771 between 2009 and 2021. Valid “S” and “P” method flask air H₂ measurements are retained for the South
772 Pole Observatory only. The “S” method flasks show contaminated H₂ at Samoa and show some
773 contamination or more variable H₂ at Utqiagvik (Barrow). The Mauna Loa H₂ in “S” method flasks will
774 be further evaluated and may be retained in future releases.

775 The Samoa and South Pole flask air measurements show similar maximum levels between 550 and 570
776 ppb and slightly higher minima at Samoa compared to the South Pole. The seasonal maxima occurs about
777 3 months earlier at Samoa than at the South Pole. The interannual variability is similar at both sites and is
778 dominated by step increases on three occasions: in 2012/2013, 2016 and 2020.



779 The Mauna Loa H_2 time series shows more short-term variability reflecting the variable latitudes covered
780 by an air mass before it is sampled at the high-altitude observatory and the strong spatial gradients for H_2
781 in the NH. The seasonal cycle amplitude at Mauna Loa is about 40 ppb with maximum levels in
782 April-May and minimum levels in December-January. The observed seasonal maxima range from 550 to
783 580 ppb and the observed seasonal minima range from 505 to 520 ppb. The NOAA measurements
784 indicate that annual mean H_2 levels at Mauna Loa after 2018 were higher than in previous years.

785 Of the four observatories, the Barrow H_2 time series shows the lowest levels and the strongest seasonal
786 cycle, about 60 ppb. The observed seasonal maximum ranges from 520 to 540 ppb in April-May and the
787 observed seasonal minimum in September-November ranges from 450 to 490 ppb.

788 Despite having larger emissions in the NH, the H_2 interhemispheric gradient shows lower levels in the
789 extratropical NH. This is related to the larger land masses in the NH and the soil sink being the dominant
790 removal process for H_2 . Warwick et al. [2022] report model-based estimates for the H_2 lifetime of 8.3
791 years for the OH sink (from the authors base model configuration) and of 2.5 years for the soil uptake
792 (average of existing literature studies). In their flux inversion, Yver et al. [2011] estimated that the NH
793 high latitudes and the tropics represent 40% and 55% of the global soil sink respectively. The soil sink
794 and OH sink in extratropical northern latitudes both peak in summertime [Price et al., 2007] leading to the
795 observed stronger H_2 minima.

796 Given the larger variability and stronger seasonality of H_2 in the NH extra tropics, it is important to look
797 at data from multiple sites to study and detect interannual and potentially long-term large-scale changes in
798 atmospheric H_2 levels. In the next section, we highlight a few features in the global network H_2 records
799 and present background air zonal mean H_2 time series based on samples collected at marine boundary
800 layer sites.

801 4.2 H_2 at the NOAA Global Cooperative Air Sampling Network Sites

802 There are 51 sites considered active or recently terminated in the Global Cooperative Air Sampling
803 Network (see map in SI Figure 8). The H_2 measurement times series for these sites are shown in SI Figure
804 9. Note that a few sites that have been discontinued are not shown in this figure. A curve fit is run for
805 each site time series based on Thoning et al. [1989]. First the code optimizes parameters for a function
806 made of a four-term harmonic and a cubic polynomial. The resulting residuals (measurements minus
807 function) are then smoothed with a low-pass filter with a 667-day cutoff and are added to the polynomial
808 part of the function to produce the “trend curve” (shown as the dark blue line in site time series plots in SI
809 Figure 9). The residuals are also smoothed with a low-pass filter with a 80 day cutoff and are added to the
810 function to produce a “smooth curve” at each site.

811 The data quality control work on our long-term measurement time series includes a data selection step
812 [Dlugokencky et al., 1994]. Samples with H_2 beyond 3.5 (4 for ASC) standard deviations of the time
813 series smoothed curve at each site are flagged as not representative of background air conditions and are
814 shown as crosses in SI Figure 9.

815 The annual mean, maximum and minimum H_2 values of the smooth curve for the 51 sites are plotted in
816 Figure 10 (in order of decreasing latitude along the x-axis) for years with retained measurements up to



817 2021. Sampling at the TPI site, on Taiping Island, Taiwan, started in May 2019, which explains the 2 (full
818 sampling year) data points for the site. Sampling at a few network sites was impacted by the covid-19
819 pandemic resulting in data gaps or delayed return shipping of samples. We recommend data users become
820 familiar with individual sampling site measurement records to best aggregate and interpret signals.

821 The interhemispheric gradient of H_2 , with higher levels in the SH, is apparent in the annual means
822 distribution across sites in Figure 10 (green circles). The majority of sites in the SH (BKT to SPO on the
823 right side of Figure 10) show smaller seasonal cycle amplitudes (<23 ppb) than NH sites; however,
824 several sites have interannual variations in their H_2 seasonal cycle amplitudes (SI Figure 9). Sites with the
825 lowest H_2 seasonal minima (Figure 10, blue x symbols) likely are the most influenced by soil uptake. A
826 few sites (for ex. TAP, AMY, LLN, CPT) show higher smooth curve annual maxima (Figure 10, red
827 crosses), likely reflecting upwind local or regional emissions.

828 Two sites, KUM and WIS, had a change of sampling location that resulted in visibly different H_2 mean
829 levels and seasonal cycle amplitudes. In mid 2018, the KUM site was moved 30 km NNW along the
830 Hawaii island SE coastline when access to a lava field bordering the ocean was lost in the eruption of the
831 Kīlauea volcano. The KUM sampling location change resulted in higher mean H_2 levels and a smaller
832 seasonal cycle. The WIS site moved 100 km SSE in Israel in early 2015. There are more instances of
833 depleted H_2 (in December-March) since the move, potentially reflecting a stronger influence of soil
834 uptake in air masses sampled at the newer location.

835 4.3 H_2 marine boundary layer global and zonal means

836 To extract large scale signals from the global air sampling network, we use the NOAA GML marine
837 boundary layer (MBL) zonal data product [Tans et al., 1989b; Dlugokencky et al., 1994]. Time series
838 from remote MBL sites are smoothed and interpolated to produce a latitude versus time surface of the H_2
839 mean MBL mole fraction (Figure 11). For H_2 , the number of sites included in the zonal mean calculations
840 ranges from 29-42 sites until July 2017 when sampling from the Pacific Ocean shipboard (POC) was
841 stopped, after which 24-27 sites were included in the calculation. Because the Global Cooperative Air
842 Sampling Network is sparse in the tropics and in the SH mid latitudes, the MBL product likely does not
843 equally detect and reflect interannual variability in fluxes in these under-sampled regions, for example
844 biomass burning emissions in Africa and South America.

845 To further isolate changes in background H_2 at different latitudes, we first calculate MBL global (and
846 zonal band) means (shown in SI Figure 10) and then derive anomalies by removing the 2010-2021
847 average year from the global (or zonal band mean) time series. Figure 12 shows the MBL anomaly for H_2
848 (black lines) and CO (dashed blue lines) for the global mean and 5 zonal band means (NH and SH Polar
849 (53-90°), NH and SH Temperate (17.5-53°) and Tropics (17.5°S to 17.5°N). The NOAA GML CO
850 measurements are for the same air samples as the H_2 measurements [Pétron et al., 2023b]. Here, we derive
851 the global and zonal means for CO using the 2009-2022 MBL CO measurements and the anomalies are
852 based on the 2010-2021 smooth curve zonal mean results to be consistent with the H_2 data analysis.

853 CO is emitted during incomplete combustion and is a useful marker of biomass burning emissions. CO
854 has a shorter atmospheric lifetime than H_2 which results in shorter-lived CO anomalies from pulse
855 emissions. The data reduction for the anomaly analysis is slightly different from Langenfelds et al. [2002]



856 investigation of CO₂, CH₄, H₂, and CO interannual variability in the CSIRO network 1992-1999 time
857 records. The CSIRO authors employed the same [Thoning et al., 1989] data smoothing technique as we
858 do but used the derivative of the trend curve to analyze correlations in interannual growth rate variations
859 between species. The anomaly approach chosen here allows to retain the timing of abrupt changes in the
860 measurement records.

861 Over 2010-2021, background air H₂ has increased at all latitudes (Figure 12). The global mean MBL H₂
862 shows a non-uniform increase over this time with a noticeable 10 ppb step increase in 2016. The global
863 mean MBL H₂ was 20.2 ±0.2 ppb higher in 2021 compared to 2010 (Figure 12a).

864 The meridional gradient and zonal band mean plots (Figure 11 and Figure 12b-f) highlight the evolution
865 of background air H₂ at different latitudes. By construction, the smooth curve anomalies are not directly
866 proportional to the biomass burning emissions that likely caused them. Rather the anomalies in the
867 smooth curves are useful to point to time periods when several successive air samples at a site show
868 similar deviations from the average seasonal cycle and multi-year trend.

869 The 2016 H₂ step increase is detected in the Tropics and SH. In the Tropics it coincides with a strong
870 positive CO anomaly that started in November 2015, reached a peak amplitude of 15 ppb mid-January
871 2016 and ended in May 2016. The 2015/2016 H₂ anomaly is first detected at Bukit Kototabang, Indonesia
872 (BKT) and later at Ascension Island (ASC), Cape Grim (CGO) and Crozet Island (CRZ) (SI Figure 11).
873 Some BKT air samples impacted by biomass burning emissions show enhancements of 100s ppb in CO
874 and H₂. The BKT CO and H₂ data also show enhancements likely related to biomass burning in 2015. The
875 2015 fire season in Indonesia was among the most intense on record as shown by remote sensing products
876 of fire counts, CO and aerosols. Field et al. [2016] found that burning activities to clear peatland for
877 farming likely contributed to larger emissions than expected from dry conditions alone in 2015.

878 There is another step increase in the Polar SH zonal band in early 2020, also coinciding with a pulse
879 anomaly in CO (Figure 12f) likely related to large wildfires in Australia in late 2019-early 2020. The
880 Cape Grim (CGO) and Crozet Island (CRZ) smoothed curves show a large jump between the late 2019
881 minimum and early 2020 maximum when the CGO CO measurement seasonal minimum is also 10-12
882 ppb higher than in other years (SI Figure 11). van der Welde et al. [2021] estimate that the 2019-2020
883 fires in Australia emitted 80% more CO₂ than “normal” Australian annual fire and fossil fuel emissions
884 combined.

885 In the NH extratropics bands, positive anomalies in H₂ in 2021 coincide with CO pulse anomalies. For the
886 Polar (Temperate) NH zonal band, the CO anomaly lasts from mid-July (June) to December 2021 with a
887 peak in September and an anomaly maximum amplitude of 37 ppb (19 ppb). Record high emissions of
888 CO₂ and CO from boreal forest fires in Eurasia and North America in 2021 have been reported by Zheng
889 et al. [2023].

890 Previously, Simmonds et al. [2005] and Grant et al. [2010] have reported on the observed variability in
891 the Mace Head continuous H₂ measurement record and linked interannual variability in the baseline
892 annual mean H₂ to larger fire emission events. More recently, Derwent et al. [2023] shared an updated
893 analysis of the February 1994-September 2022 Mace Head in-situ H₂ measurements. The in situ record
894 shows higher monthly mean baseline H₂ levels in recent years and the authors report an increase in



895 monthly mean anomalies after December 2015 (slope of 2.4 ± 0.5 ppb/yr). They postulate that a
896 “missing” source of increasing intensity after 2010 may be behind the observed sustained increased H_2 ,
897 which is markedly different from the 1998-1999 anomalies attributed to biomass burning. Derwent et al.
898 [2023] explore potential candidates for the missing sources. However, in the absence of strong and
899 quantitative direct evidence at this time, additional studies are needed to interpret the observed H_2
900 variability.

901 5. Conclusions

902 In this paper, we have described how NOAA GML has adopted the MPI X2009 H_2 calibration scale. The
903 work was confined to measurements on GC-HePDD instruments. The GML H_2 primary standards in
904 electropolished stainless steel cylinders have been calibrated once by the MPI CCL in Fall 2020. We have
905 used the CCL assignments to propagate the scale to secondary and tertiary standards. H_2 increases in
906 most air standards stored in aluminum cylinders. A curve fit is applied to each standard calibration history
907 to determine a time-dependent H_2 assignment on MPI X2009. The tertiary and working standards H_2
908 assignments were then used to reprocess results for NOAA flask air H_2 measurements on MPI X2009.
909 These NOAA Global Cooperative Air Sampling Network flask reprocessed H_2 measurements for
910 2009-2021 are now publicly available [Pétron et al., 2023a]. For the period 2010-2021, same air
911 measurements with GAW partner laboratories have annual mean differences less than 2 ppb for the Cape
912 Grim comparison with CSIRO and less than 3 ppb for the Ochsenkopf comparison with MPI BGC. Over
913 2010-2021, background air H_2 has increased at all latitudes. However, site time series and marine
914 boundary layer H_2 zonal means show significant interannual variability. We find that some of strongest H_2
915 zonal mean anomalies coincide with CO anomalies and therefore were likely driven by large biomass
916 burning events in Indonesia (2015), Australia (2019/2020), and boreal latitudes (2012 and 2021) [Field et
917 al., 2016; Petetin et al., 2018; Zheng et al., 2023]. A full analysis of the NOAA Global Cooperative Air
918 Sampling Network H_2 measurement records is beyond the scope of this paper. This dataset complements
919 WMO/GAW partner laboratories H_2 measurements and it will be updated and extended routinely
920 moving forward.

921

922 Data and Code Availability

923 The NOAA global network flask air H_2 and CO time series are available at

924 <https://doi.org/10.15138/WP0W-EZ08>.

925

926 We kindly request that users of the NOAA H_2 dataset cite:

927 Pétron, G., Crotwell, A., Crotwell, M., Kitzis, D., Madronich, M.,

928 Mefford, T., Moglia, E., Mund, J., Neff, D., Thoning, K., & Wolter, S.

929 (2023). Atmospheric Hydrogen Dry Air Mole Fractions from the NOAA GML Carbon

930 Cycle Cooperative Global Air Sampling Network, 2009-2021 [Data set].

931 NOAA GML CCGG Division. Version: 2023-05-25, <https://doi.org/10.15138/WP0W-EZ08>

932

933 The python class used to filter and smooth time series data is available and explained at:

934 <https://gml.noaa.gov/aftp/user/thoning/ccgcrv/ccgfilt.pdf> and the method can be referenced as

935 [Thoning et al., 1989].



936

937 **Supplement**

938 The supplement for this article is available in a separate file.

939

940 **Author Contributions**

941 GP and AC designed the scale revision work. GP, AC and JM implemented the scale revision.
942 GP, AC, MC, MM, DN and JM contributed to the data quality control. GP and JP analyzed
943 network site time series. AC designed, built and oversaw the H₂ calibration scale transfer and the
944 flask air analysis system operations, working with Paul Novelli until he retired in 2017. TM and
945 AC carried out tank calibrations. BH prepared the primary standards. DK was in charge of the
946 whole air secondary and tertiary standards preparation. MM and EM were responsible for the
947 flask air analysis lab operations, working with Patricia Lang until her retirement in 2019. EM
948 managed the flask logistics laboratory and flask metadata entries. DN with support from SW
949 managed the NOAA Global Air Sampling Network. DN managed sampling equipment for sites.
950 JM manages the database and data releases, JM, KT and AC developed code and user interfaces
951 for data processing, quality control and exploration. AJ calibrated the NOAA primary standards.
952 AJ, PK and RL contributed data from their measurement programs. GP prepared the manuscript
953 with contributions from AC and AJ and edits from BH, MC, RL, and JP.

954

955 **Competing Interests**

956 The authors declare that they have no conflict of interest.

957

958 **Acknowledgements**

959 We are grateful for our partners worldwide who collect and ship flask air samples to NOAA GML,
960 Boulder, CO for analysis. We thank past and current NOAA GML and CU CIRES colleagues for their
961 contributions to the network operations, measurements, data management and data quality control. Gary
962 Morris and Kathryn McKain provided valuable comments on the manuscript.

963

964 **Financial support**

965 This research was supported in part by NOAA cooperative agreements NA17OAR4320101 and
966 NA22OAR4320151.

967

968

969



970 References

- 971 Bertagni, M.B., Pacala, S.W., Paulot, F. et al. Risk of the hydrogen economy for atmospheric methane.
972 *Nat Commun* 13, 7706, doi: 10.1038/s41467-022-35419-7, 2022.
- 973 Brito J., Wurm, F., Yáñez-Serrano, A. M., de Assunção, J. V., Godoy, J. M., and Artaxo, P., Vehicular
974 Emission Ratios of VOCs in a Megacity Impacted by Extensive Ethanol Use: Results of Ambient
975 Measurements in São Paulo, Brazil, *Environmental Science & Technology*, 49 (19), 11381-11387, doi:
976 10.1021/acs.est.5b03281, 2015.
- 977 Ciais P., Tans, P. P., Trolier, M., et al., A Large Northern Hemisphere Terrestrial CO₂ Sink Indicated by
978 the ¹³C/¹²C Ratio of Atmospheric CO₂. *Science* 269,1098-1102, doi: 10.1126/science.269.5227.1098,
979 1995.
- 980 Conway, T. J., Tans, P. P., Waterman, L. S., Thoning, K. W., Kitzis, D. R., Masarie, K. A., and Zhang, N.,
981 Evidence for interannual variability of the carbon cycle from the National Oceanic and Atmospheric
982 Administration/Climate Monitoring and Diagnostics Laboratory Global Air Sampling Network, *J.*
983 *Geophys. Res.*, 99(D11), 22831–22855, doi:10.1029/94JD01951, 1994.
- 984 Cooper O.R., Schultz M. G., Schröder S., et al.; Multi-decadal surface ozone trends at globally distributed
985 remote locations. *Elementa: Science of the Anthropocene*; doi:10.1525/elementa.420, 2020.
- 986 de Kleijne, K., de Coninck H., van Zelm, R., Huijbregts M. A., and V. Hanssen S. V., The many
987 greenhouse gas footprints of green hydrogen, *Sustainable Energy Fuels*, 6, 4383-4387, doi:
988 10.1039/D2SE00444E, 2022.
- 989 Derwent, R. G., Simmonds, P. G., O'Doherty, S., Manning, A. J., Spain, T. G., High-frequency,
990 continuous hydrogen observations at Mace Head, Ireland from 1994 to 2022: Baselines, pollution events
991 and 'missing' sources, *Atmospheric Environment*, Volume 312, doi: 10.1016/j.atmosenv.2023.120029,
992 2023.
- 993
- 994 Dlugokencky, E. J., Steele, L. P., Lang, P. M., and Masarie, K. A., The growth rate and distribution of
995 atmospheric methane, *J. Geophys. Res.*, 99(D8), 17021– 17043, doi:10.1029/94JD01245, 1994.
996
- 997 Dlugokencky, E. J., Bruhwiler, L., White, J. W. C., et al., Observational constraints on recent increases in
998 the atmospheric CH₄ burden, *Geophys. Res. Lett.*, 36, L18803, doi:10.1029/2009GL039780, 2009.
999
- 1000 Field, R. D., van der Werf, G. R., Fanin, T., et al., Indonesian fire activity and smoke pollution in 2015
1001 show persistent nonlinear sensitivity to El Niño-induced drought. *Proceedings of the National Academy*
1002 *of Sciences* 113, 33(2016), 9204–9209, doi: 10.1073/pnas.1524888113, 2016.



1003

1004 Francey, R. J.; Steele, L. P.; Langenfelds, R. L.; and B.C. Pak, High Precision Long-Term Monitoring of
1005 Radiatively Active and Related Trace Gases at Surface Sites and from Aircraft in the Southern
1006 Hemisphere Atmosphere, *Journal of Atmospheric Sciences*, pp. 279-285,
1007 [https://doi.org/10.1175/1520-0469\(1999\)056%3C0279:HPLTMO%3E2.0.CO;2](https://doi.org/10.1175/1520-0469(1999)056%3C0279:HPLTMO%3E2.0.CO;2), 1999.

1008

1009 Francey, R. J.; Steele, L. P.; Spencer, D. A.; Langenfelds, R. L.; Law, R. M.; Krummel, P. B.; Fraser, P. J.;
1010 Etheridge, D. M.; Derek, N.; Coram, S. A.; Cooper, L. N.; Allison, C. E.; Porter, L.; Baly, S. The CSIRO
1011 (Australia) measurement of greenhouse gases in the global atmosphere. In: Report of the eleventh
1012 WMO/IAEA Meeting of Experts on Carbon Dioxide Concentration and Related Tracer Measurement
1013 Techniques; 2001; Tokyo, Japan. World Meteorological Organization; pp. 97-106.
1014 <http://hdl.handle.net/102.100.100/194315>, 2003. Last accessed December 29, 2023.

1015

1016 Friedlingstein, P., et al., Global Carbon Budget 2022, *Earth Syst. Sci. Data*, 14, 4811–4900,
1017 <https://doi.org/10.5194/essd-14-4811-2022>, 2022.

1018

1019 Grant, A., Witham, C. S., Simmonds, P. G., Manning, A. J., and O'Doherty, S.: A 15 year record of
1020 high-frequency, in situ measurements of hydrogen at Mace Head, Ireland, *Atmos. Chem. Phys.*, 10,
1021 1203–1214, doi: 10.5194/acp-10-1203-2010, 2010.

1022

1023 Heiskanen, J. et al., The Integrated Carbon Observation System in Europe. *Bulletin of the American
1024 Meteorological Society* 103 (3), pp. E855 - E872, doi: 10.1175/BAMS-D-19-0364.1, 2022.

1025

1026 Hydrogen Council and McKinsey & Company, *Hydrogen Insights 2023*, 23pp. Accessible at:
1027 <https://hydrogencouncil.com/wp-content/uploads/2023/12/Hydrogen-Insights-Dec-2023-Update.pdf>,
1028 2023. Last accessed December 29, 2023.

1029

1030 International Energy Agency, *Global Hydrogen Review 2022*, IEA, Paris,
1031 <https://www.iea.org/reports/global-hydrogen-review-2022>, License: CC BY 4.0, 284pp, 2022. Last
1032 accessed December 29, 2023.

1033

1034 Jordan, A. and Steinberg, B.: Calibration of atmospheric hydrogen measurements, *Atmos. Meas. Tech.*, 4,
1035 509–521, doi: 10.5194/amt-4-509-2011, 2011.

1036

1037 Khalil, M. A. K., and Rasmussen, R. A., Seasonal cycles of hydrogen and carbon monoxide in the polar
1038 regions: Opposite phase relationships, *Ant. J. U. S.*, 23(5), 177-178, 1989.

1039

1040 Khalil, M. A. K. and Rasmussen, R. A., Global increase of atmospheric molecular hydrogen. *Nature* 347,
1041 743–745, doi: 10.1038/347743a0, 1990.

1042

1043 Kitzis, D., *Preparation and Stability of Standard Reference Air Mixtures*, 2017.

1044 <https://gml.noaa.gov/ccl/airstandard.html>. Last accessed May 17, 2023.

1045



- 1046 Komhyr, W. D., R. H. Gammon, T. B. Harris, L. S. Waterman, T. J. Conway, W. R. Taylor, and K. W.
1047 Thoning, Global atmospheric CO₂ distribution and variations from 1968–1982 NOAA/GMCC CO₂ flask
1048 sample data, *J. Geophys. Res.*, 90(D3), 5567–5596, doi:10.1029/JD090iD03p05567, 1985.
1049
- 1050 Langenfels, R. L., Francey, R. J., Pak, B. C., Steele, L. P., Lloyd, J., Trudinger, C. M., and Allison, C. E.,
1051 Interannual growth rate variations of atmospheric CO₂ and its $\delta^{13}\text{C}$, H₂, CH₄, and CO between 1992 and
1052 1999 linked to biomass burning, *Global Biogeochem. Cycles*, 16(3), 1048, doi:10.1029/2001GB001466,
1053 2002.
1054
- 1055 Longden T., Beck, F. J., Jotzo, F., Andrews, R., Prasad, M., ‘Clean’ hydrogen? – Comparing the emissions
1056 and costs of fossil fuel versus renewable electricity based hydrogen, *Applied Energy*, Volume 306, Part B,
1057 118145, ISSN 0306-2619, doi: 10.1016/j.apenergy.2021.118145, 2022.
1058
- 1059 Masarie, K. A., Langenfels, R. L., Allison, C.E., et al., NOAA/CSIRO Flask Air Intercomparison
1060 Experiment: A strategy for directly assessing consistency among atmospheric measurements made by
1061 independent laboratories, *J. Geophys. Res.*, 106(D17), 20445–20464, doi:10.1029/2000JD000023, 2001.
1062
- 1063 Montzka, S.A., Dutton, G.S., Yu, P. et al. An unexpected and persistent increase in global emissions of
1064 ozone-depleting CFC-11. *Nature* 557, 413–417, doi: 10.1038/s41586-018-0106-2, 2018.
1065
- 1066 Novelli, P. C., Elkins, J.W., Steele, L. P., The Development and Evaluation of a Gravimetric Reference
1067 Scale For Measurements of Atmospheric Carbon Monoxide, *J. Geophys. Res.*, 96, 13,109-13,121, doi:
1068 10.1029/91JD01108, 1991.
1069
- 1070 Novelli, P. C., Steele, L. P., and Tans, P. P., Mixing ratios of carbon monoxide in the troposphere, *J.*
1071 *Geophys. Res.*, 97, 20,731-20,750, doi:10.1029/92JD02010, 1992.
1072
- 1073 Novelli, P. C., Lang, P. M., Masarie, K. A., Hurst, D. F., Myers, R., and W., E. J.: Molecular hydrogen in
1074 the troposphere: Global distribution and budget, *J. Geophys. Res.*, 104, 30427–30444, doi:
1075 10.1029/1999JD900788, 1999.
1076
- 1077 Novelli, P. C., Crotwell, A. M., and Hall, B. D., Application of Gas Chromatography with a Pulsed
1078 Discharged Helium Ionization Detector for Measurements of Molecular Hydrogen, *Env. Sci. Technol.*
1079 (43), 2431-2436, doi: 10.1021/es803180g, 2009.
1080
- 1081 Ocko, I. B. and Hamburg, S. P.: Climate consequences of hydrogen emissions, *Atmos. Chem. Phys.*, 22,
1082 9349–9368, doi: 10.5194/acp-22-9349-2022, 2022.
1083
- 1084 Oltmans S. J. and Levy, H. II, Surface ozone measurements from a global network,
1085 *Atmospheric Environment*, Volume 28, Issue 1, Pages 9-24, ISSN 1352-2310, doi:
1086 10.1016/1352-2310(94)90019-1, 1994.
1087
- 1088 Petetin, H., Sauvage, B., Parrington, M., Clark, H., Fontaine, A., Athier, G., Blot, R., Boulanger, D.,
1089 Cousin, J.-M., Nédélec, P., and Thouret, V.: The role of biomass burning as derived from the



- 1090 tropospheric CO vertical profiles measured by IAGOS aircraft in 2002–2017, *Atmos. Chem. Phys.*,
1091 18, 17277–17306, doi: 10.5194/acp-18-17277-2018, 2018.
- 1092
- 1093 Pétron, G., Crotwell, A., Crotwell, M., Kitzis, D., Madronich, M., Mefford, T., Moglia, E., Mund, J., Neff,
1094 D., Thoning, K., & Wolter, S., Atmospheric Hydrogen Dry Air Mole Fractions from the NOAA GML
1095 Carbon Cycle Cooperative Global Air Sampling Network, 2009–2021 [Data set]. NOAA GML CCGG
1096 Division. Version: 2023-05-25, doi: 10.15138/WP0W-EZ08, 2023a.
- 1097
- 1098 Pétron G., A.M. Crotwell, M.J. Crotwell, E. Dlugokencky, M. Madronich, E. Moglia, D. Neff, K.
1099 Thoning, S. Wolter, J.W. Mund, Atmospheric Carbon Monoxide Dry Air Mole Fractions from the
1100 NOAA GML Carbon Cycle Cooperative Global Air Sampling Network, 1988–2022, Version:
1101 2023-08-28, doi: 10.15138/33bv-s284, 2023b.
- 1102
- 1103 Price, H., Jaegle, L., Rice, A., Quay, P., Novelli, P. C., and Gammon, R.: Global budget of molecular
1104 hydrogen and its deuterium content: Constraints from ground station, cruise, and aircraft observations, *J.*
1105 *Geophys. Res.*, 112, D22108, doi:10.1029/2006JD008152, 2007.
- 1106
- 1107 Propper, R., Wong, P., Bui, S., Austin, J., Vance, W., Alvarado, Á., Croes, B., and Luo, D., Ambient and
1108 Emission Trends of Toxic Air Contaminants in California, *Environmental Science & Technology*, 49 (19),
1109 11329–11339, doi: 10.1021/acs.est.5b02766, 2015.
- 1110
- 1111 Schultz, M.G., Akimoto, H., Bottenheim, J., et al., The Global Atmosphere Watch reactive gases
1112 measurement network. *Elementa: Science of the Anthropocene*, 3, doi:
1113 10.12952/journal.elementa.000067, 2015.
- 1114
- 1115 Simmonds, P. G., Derwent, R. G., O’Doherty, S., Ryall, D. B., Steele, L. P., Langenfelds, R. L., Salameh,
1116 P., Wang, H. J., Dimmer, C. H., and Hudson, L. E.: Continuous high-frequency observations of hydrogen
1117 at the Mace Head baseline atmospheric monitoring station over the 1994–1998 period, *J. Geophys. Res.*,
1118 105, 12105–12121, doi: 10.1029/2000JD900007, 2000.
- 1119
- 1120 Simmonds, P. G., A.J. Manning, R.G. Derwent, P. Ciais, M. Ramonet, V. Kazan, D. Ryall,
1121 A burning question. Can recent growth rate anomalies in the greenhouse gases be attributed to large-scale
1122 biomass burning events?, *Atmospheric Environment*, Volume 39, Issue 14, Pages 2513–2517, doi:
1123 10.1016/j.atmosenv.2005.02.018, 2005.
- 1124
- 1125 Simpson, I.J., M.P.S. Andersen, S. Meinardi, L. Bruhwiler, N.J. Blake, et al., Long-term decline of global
1126 atmospheric ethane concentrations and implications for methane. *Nature*, 488(7412):490–494, doi:
1127 10.1038/nature11342, 2012.
- 1128
- 1129 Steele, L.P., Fraser, P.J., Rasmussen, R.A. et al. The global distribution of methane in the troposphere. *J*
1130 *Atmos Chem* 5, 125–171, doi: 10.1007/BF00048857, 1987.
- 1131



- 1132 Storm, I., Karstens, U., D'Onofrio, C., Vermeulen, A., and Peters, W.: A view of the European carbon flux
1133 landscape through the lens of the ICOS atmospheric observation network, *Atmos. Chem. Phys.*, 23,
1134 4993–5008, doi: 10.5194/acp-23-4993-2023, 2023.
- 1135 Tans, P.P., Thoning, K.W., Elliot, W.P., and Conway, T.J., *Background atmospheric CO₂ patterns from*
1136 *weekly flask samples at Barrow, Alaska: Optimal signal recovery and error estimates*, NOAA Tech.
1137 Memo. (ERL-ARL-173). Environ. Res. Lab., Boulder, Colo., 131 pp. 1989a.
- 1138 Tans, P.P., T.J. Conway, and T. Nakazawa, Latitudinal distribution of the sources and sinks of atmospheric
1139 carbon dioxide derived from surface observations and an atmospheric transport model, *J. Geophys. Res.*,
1140 94, 5151–5172, doi: 10.1029/JD094iD04p05151, 1989b.
- 1141 Thompson A. M., J. C. Witte, S. J. Oltmans, F. J. Schmidlin, SHADOZ - A tropical
1142 ozonesonde-radiosonde network for the atmospheric community. *Bulletin of the American Meteorological*
1143 *Society*, Vol. 85, No. 10, pp. 1549–1564, <http://www.jstor.org/stable/26221206>, 2004.
- 1144 Thoning, K.W., P.P. Tans, and W.D. Komhyr, Atmospheric carbon dioxide at Mauna Loa Observatory 2.
1145 Analysis of the NOAA GMCC data, 1974–1985, *J. Geophys. Res.*, 94, 8549–8565, doi:
1146 10.1029/JD094iD06p08549, 1989.
- 1147 Tørseth, K., Aas, W., Breivik, K., Fjæraa, A. M., Fiebig, M., Hjellbrekke, A. G., Lund Myhre, C.,
1148 Solberg, S., and Yttri, K. E.: Introduction to the European Monitoring and Evaluation Programme
1149 (EMEP) and observed atmospheric composition change during 1972–2009, *Atmos. Chem. Phys.*, 12,
1150 5447–5481, doi: 10.5194/acp-12-5447-2012, 2012.
- 1151 van der Velde, I.R., van der Werf, G.R., Houweling, S. *et al.* Vast CO₂ release from Australian fires in
1152 2019–2020 constrained by satellite. *Nature* 597, 366–369, doi: 10.1038/s41586-021-03712-y, 2021.
- 1153 von Schneidmesser E., Monks, P.S., Plass-Duelmer C., Global comparison of VOC and CO observations
1154 in urban areas, *Atmospheric Environment*, Volume 44, Issue 39, Pages 5053–5064, ISSN 1352-2310, doi:
1155 10.1016/j.atmosenv.2010.09.010, 2010.
- 1156 Yver, C. E., Pison, I. C., Fortems-Cheiney, A., A new estimation of the recent tropospheric molecular
1157 hydrogen budget using atmospheric observations and variational inversion, *Atmos. Chem. Phys.*, 11,
1158 3375–3392, doi: 10.5194/acp-11-3375-2011, 2011.
- 1159 Warwick, N., Griffiths, P., Keeble, J., Archibald A., Pyle, J., and Shine, K.: Atmospheric implications of
1160 increased Hydrogen use, UK government's Department of Business, Energy and Industrial Strategy
1161 (BEIS) report, 2022. Accessible at:
1162 <https://assets.publishing.service.gov.uk/media/624eca7fe90e0729f4400b99/atmospheric-implications-of-i>
1163 [ncreased-hydrogen-use.pdf](https://assets.publishing.service.gov.uk/media/624eca7fe90e0729f4400b99/atmospheric-implications-of-increased-hydrogen-use.pdf), Last accessed: October 18, 2023.
- 1164 World Meteorological Organization, Global Atmospheric Watch, 20th WMO/IAEA Meeting on Carbon
1165 Dioxide, Other Greenhouse Gases and Related Measurement Techniques (GGMT-2019), report 255,
1166 2020. Accessible at:



1167 [https://library.wmo.int/records/item/57135-20th-wmo-iaea-meeting-on-carbon-dioxide-other-greenhouse-](https://library.wmo.int/records/item/57135-20th-wmo-iaea-meeting-on-carbon-dioxide-other-greenhouse-gases-and-related-measurement-techniques-ggmt-2019)
1168 [gases-and-related-measurement-techniques-ggmt-2019](https://library.wmo.int/records/item/57135-20th-wmo-iaea-meeting-on-carbon-dioxide-other-greenhouse-gases-and-related-measurement-techniques-ggmt-2019). Last accessed: December 4, 2023.

1169 World Meteorological Organization, Greenhouse Gas Bulletin (18): The State of Greenhouse Gases in the
1170 Atmosphere Based on Global Observations through 2021. 10p., 2022. Accessible at:

1171 <https://library.wmo.int/idurl/4/58743>. Last accessed: January 2, 2024.

1172 Worthy, D. E. J., Rauh, M. K., Huang, L., et al., Results of a Long-Term International Comparison of
1173 Greenhouse Gas and Isotope Measurements at the Global Atmosphere Watch (GAW) Observatory in
1174 Alert, Nunavut, Canada, *Atmos. Meas. Tech.*, 16, 5909–5935, doi: 10.5194/amt-16-5909-2023, 2023.

1175 Yap, J., and McLellan B. A., Historical Analysis of Hydrogen Economy Research, Development, and
1176 Expectations, 1972 to 2020, *Environments*, 10, 11, doi: 10.3390/environments10010011, 2023.

1177 Zheng, B., Ciais, P., Chevallier, F., et al., Record-high CO₂ emissions from boreal fires in 2021. *Science*,
1178 379, 912–917, doi: 10.1126/science.ade0805, 2023.

1179



1180 Tables

1181

1182 Table 1. NOAA GML H₂ primary standards (prepared gravimetrically) and their WMO/MPI X2009

1183 assignments. All H₂ dry air mole fractions and their uncertainties are in ppb.

Serial Number	Fill code	Fill Date	CCL value	CCL uncertainty
SX-3558	A	2008-10-17	248.4	0.1
SX-0614470	A	2019-04-15	352.8	0.1
SX-3543	B	2008-11-03	425.4	0.2
SX-3540	B	2007-08-07	488	0.2
SX-0614471	A	2019-04-19	496.5	0.3
SX-3523	C	2007-07-24	527	0.2
SX-3554	A	2007-08-02	601.2	0.2
SX-0614472	A	2019-04-19	701.9	0.2

1184

1185

1186 Table 2: H₂ secondary standards used in the tank calibration laboratory and H₂ tertiary standards used on

1187 the MAGICC-1 and MAGICC-2 systems (2009 to 2019).

Tank Calibration / H9								
Tank ID (fill)	Time of use	t0	Assignment at t0 (ppb)	C1 (ppb/yr)	C2 (ppb/yr ²)	N	Residuals standard deviation (ppb)	Fill date
CC119811 (A)	2/05/2008 to 6/02/2013	2010.0689	549.4	2.0	0	47	0.50	2006-01-01 SM*
CA03233 (B)	6/02/2013 to 11/01/2018	2016.7106	502.8	0	0	19	0.23	2010-08-12 NWR
MAGICC-1 / H11								
Tank ID (fill)	Time of use	t0	Assignment at t0 (ppb)	C1 (ppb/yr)	C2 (ppb/yr ²)	N	Assignment uncertainty (ppb)**	Fill date
CA08107 (D)	7/22 to 8/7/2019	2019.2959	562.9	15.4	0	6	0.6	2018-11-09 NWR
CB11090 (B)	10/18/2018 to 7/19/2019	2019.1482	576.3	6.9	0	4a	0.6 After 2019-06-21: 1.5	2016-9-30 NWR
CB11551 (A)	2/13 to 10/17/2018	2018.1878	548.8	6.7	0	3a,b, c	0.5 After 2018-08-27: 1.5	2015-1-01 SM*
CC91285 (C)	6/19/2017 to 2/13/2018	2017.1711	538.4	0	0	8	0.5	2015-8-14 NWR
CA08165	10/13/2016 to	2016.9137	535.7	4.5	0	3c	0.5	2011-12-16



(B)	06/16/2017							NWR
CC302566 (B)	3/21/2016 to 10/12/2016	2016.3645	540.2	4.4	0	5	0.5	2015-8-14 NWR
CC105491 (B)	8/10/2015 to 3/18/2016	2015.1506	522.3	0	0	5d	1.0	2014-1-16 NWR
ND33801 (B)	8/4/2014 to 8/7/2015	2013.8771	509.3	0.9	0	6e	0.5 After 2015-05-14: 1.0	2012-12-27 NWR
CB09117 (A)	2/18 to 8/1/ 2014	2013.8912	635.3	28.7	0	5	2	2012-12-17 SM
ND46735 (A)	9/10/2012 to 2/13/2014	2012.9158	527.4	2.5	-1.0	7e,f	0.5 After 2013-12-11: 1.0	2011-1-1 estimated
CA04505 (B)	12/9/2011 to 9/7/2012	2011.4593	540.6	1.7	0	3c,d	1.0	2010-8-12 NWR
ND38963 (A)	8/12/2010 to 12/7/2011	2011.704	586.0	6.2	0	4	0.5	2009-1-1 estimated
CC71649 (E)	1/22 to 8/6 2010	2009.1184	507.1	8.4	0	7b,e	1.5	2008-9-19
MAGICC-2 / H8								
Tank ID (fill)	Time of use		Assignment at t0 (ppb)	C1	C2	N	Assignment uncertainty (ppb)**	Fill date
ND38954 (B)	3/26/2013 to 3/21/2014	2014.2094	516.6	2.0	0	5	0.5	2012-12-9 NWR
CA03409 (B)	5/23/2011 to 3/25/2013	2011.6278	526.6	0	0	5e	0.5 After 2013-01-21: 1.0	2010-1-1 estimated
ND38415 (A)	4/5/2010 to 5/20/2011	2010.2502	566.1	20.9	-8.7	6	0.5	2009-1-1 estimated
CC305198 (A)	11/2//2009 to 4/3/2010	2009.7211	557.9	65.8	0	3a,b	1.5 After 2010-01-31: 2.5	2009-1-1 SM*

1188 * Gravimetric blends with CO, H₂, CO₂, CH₄ and N₂O in zero air purchases from Scott Marrin.

1189 ** Uncertainty estimates listed for the tertiary standard assignments assume a 0.5 ppb uncertainty for each

1190 calibration result on H9 and do not formally include the uncertainty on the secondary standard

1191 assignments.

1192 a. Assignment does not use existing post-use calibration results that show larger drift

1193 b. Drift change towards end of use, additional drift correction applied.

1194 c. Force linear fit in drift calculation code

1195 d. Only predeployment calibrations

1196 e. No end-of-use or post-use calibration

1197 f. Force quadratic fit in drift calculation code



1198 Table 3: H₂ working standards used on the MAGICC-3 system. Best polynomial curve fit coefficients to
 1199 the August 2019–December 2022 calibration histories.

Tank ID (fill)	t0	Assignment at t0 (ppb)	C1 (ppb/yr)	C2 (ppb/yr ²)	N	Assignment uncertainty (ppb)	Fill date
CA01414 (I)	2020.0964	238.4	10.0	-1.9	9	0.5 ppb	2017-12-29 NWR
CA04403 (F)	2020.1052	474.6	10.2	-1.7	9	0.5 ppb	2017-12-1 NWR
CB11270 (A)	2020.0012	515.0	2.9	-0.5	9	0.5 ppb	2017-12-1 NWR
CA06388 (H)	2019.9423	551.2	1.1	0	9	0.5 ppb	2018-2-23 NWR
CA05773 (F)	2020.2585	565.6	1.4	0	8	0.5 ppb	2018-5-17 NWR
CB11034 (B)	2020.0783	580.1	8.3	-1.2	9	0.5 ppb	2018-5-17 NWR
CA05680 (H)	2020.0904	588.1	1.9	0	9	0.5 ppb	2017-12-1 NWR
CB11405 (C)	2020.1474	605.6	23.3	-1.6	9	0.5 ppb	2018-5-17 NWR

1200

1201

1202

1203



1204 Table 4: H9 Target air tanks with zero or linear growth in H₂

Linear Drift Rate (ppb/yr)	Target Tank IDs	Standard deviation of residuals to best fits (ppb)
0	CA05278, CA06194, CA08247, CC121971, CC311842 ND16439, ND33960	0.46
0-1	ALM-065166, CA05300, CC71607, CC73110	0.42
2-5	CA04551, CA07328, CB10910	0.32
5-10	CC71579	0.36
> 20	CA08145	0.48

1205

1206

1207



1208 Table 5. Summary statistics for H₂ differences between test air tank-fill assignment (based on H9
 1209 calibration history) and associated TST flask measurements on MAGICC systems

System / Instrument	Test air tank id and fill	Differences mean (ppb)	Differences standard deviation (ppb)	Number of samples
MAGICC-2 / H8	AL43-113 D, E	-0.3	1.3	528
MAGICC-1 / H11	AL43-113 D, E, G	+0.3	1.1	1231
MAGICC-3 / H8	AL47-145 G	-0.9	1.5	388
MAGICC-3 / H11	AL43-113 G	+0.4	0.6	144

1210

1211

1212

1213 Table 6. Summary statistics for SPO flask pair H₂ differences. Npairs= Number of flask pairs.

System/ Instrument	SPO "P" flasks Absolute differences			SPO "S" flasks Absolute differences			SPO "S"- "P" Pair mean differences		
	Mean (ppb)	Std dev (ppb)	Npairs	Mean (ppb)	Std dev (ppb)	Npairs	Mean (ppb)	Std dev (ppb)	Npairs
MAGICC-2 / H8	1.3	1.0	165	1.1	0.9	87	-0.4	1.5	81
MAGICC-1 / H11	0.9	0.8	292	0.9	0.8	143	-0.2	1.3	144
MAGICC-3 / H8	1.6	1.3	45	1.2	1.2	25	-0.1	1.7	25
MAGICC-3 / H11	0.7	0.6	76	0.8	0.6	35	-0.5	0.8	43

1214

1215

1216



1217 Table 7: Annual mean of H₂ measurement differences for air samples from the Cape Grim Observatory
 1218 (CGO), Ochsenkopf (OXK) and Alert (ALT). Non background air sample measurement results are
 1219 included. Collocated (not same air) samples at ALT are matched within a +/- 60 minutes window.
 1220 [updated 9-25-23]
 1221

Year	NOAA ICP-NOAA nonICP		CGO NOAA non ICP minus CSIRO ICP	OXK NOAA ICP minus MPI ICP	ALT NOAA minus CSIRO (not same air)	ALT NOAA minus MPI (not same air)
	CGO*	OXK				
2010	-	-0.05	0.72	-0.17	-3.4	-3.5
2011	-	0.15	0.50	-0.02	2.2	-3.9
2012	0.58	0.13	0.40	-0.29	0.66	-2.3
2013	-	0.01	0.23	0.80	1.30	-1.4
2014	-	0.19	1.37	1.61	0.63	-1.1
2015	-	0.85	0.02	0.53	0.52	-1.4
2016	1.32	0.20	1.54	2.91	-0.32	-1.4
2017	1.19	0.56	1.38	2.49	3.2	-
2018	0.91	0.53	1.31	1.69	1.2	-1.3
2019	0.73	-0.07	0.30	1.25	1.0	-0.81
2020	0.18	na	0.19	-	0.01	-0.22
2021	0.33	0.33	0.86	1.71	3.4	-

1222 *Most NOAA ICP flasks from CGO had a small contamination for CO and H₂ prior to 2019. If the
 1223 NOAA ICP flask H₂ results are > 2ppb larger than the NOAA non-ICP flask H₂ in the pair, the ICP flask
 1224 H₂ has been rejected. Only years with at least 10 valid H₂ pairs are included.



1225 Table 8: Flask air H₂ measurement uncertainty components

Uncertainty components	1 sigma uncertainty estimate (ppb)	Source
Tertiary standard time-dependent assignment uncertainty (1 point calibration)	0.5-2.5 Tank specific (see Table 2)	Calibration histories, residuals to best fit, TST flasks
MAGICC-3 response curve uncertainty	0.5	Preliminary estimate, will be reassessed.
Measurement repeatability on H8	1.3 (MAGICC-2) 1.5 (MAGICC-3)	TST and SPO flask pair differences (Tables 5 and 6)
Measurement repeatability on H11	1.1 (MAGICC-1) 0.6 (MAGICC-3)	

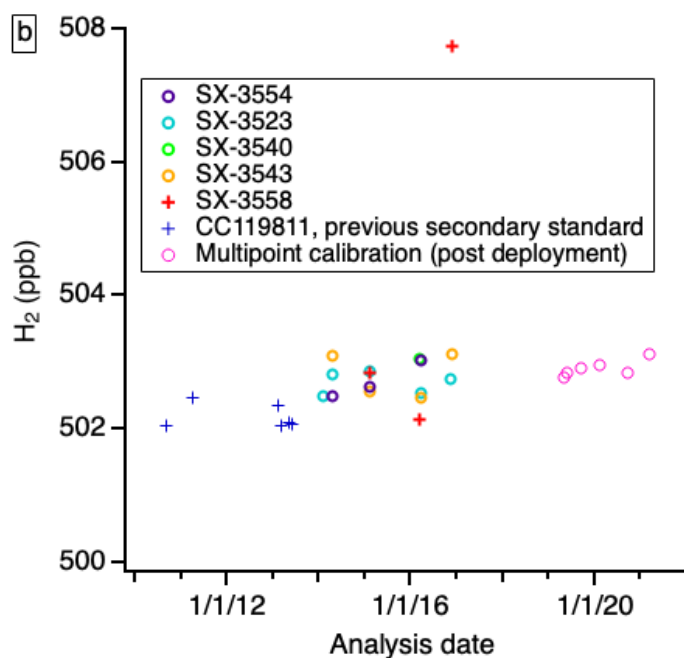
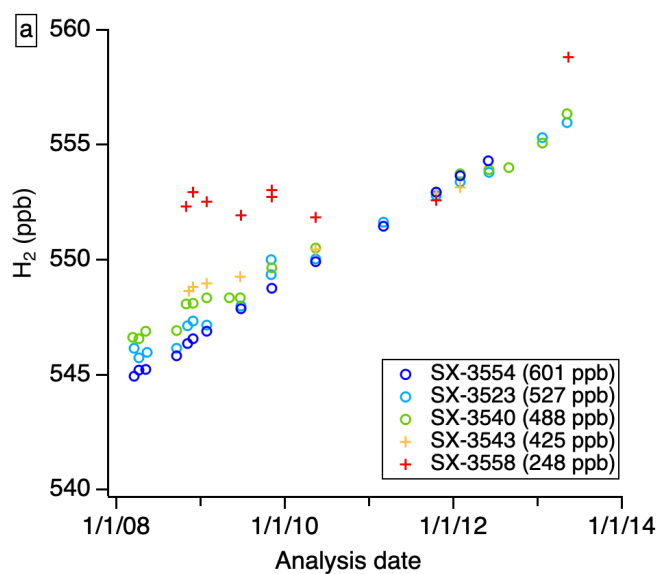
1226



1227 Figures

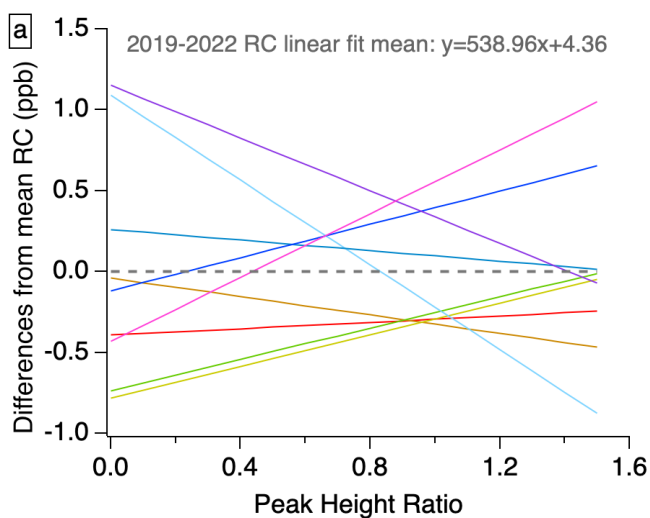
1228

1229 Figure 1. Calibration results for GML two H₂ secondary standards (a) CC119811 and b) CA03233) on H9
1230 against one of the primary standards. 2019-2020 multipoint calibration results on H9 are also shown for
1231 CA03233 (pink circles). Only results shown with open circles are used for the assignments.

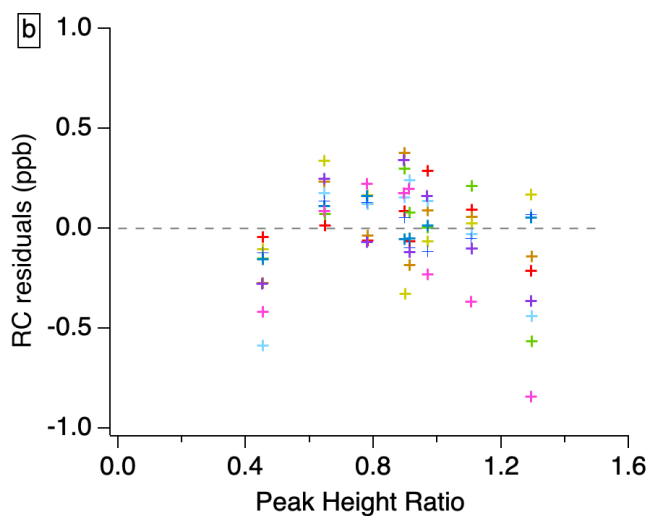




1235 Figure 2: 2019-2022 H9 standard calibration response curve (RC) results: a) differences from the mean
1236 RC linear fit mean and b) residuals of the response curve fits. Different colors are for different calibration
1237 episodes.
1238



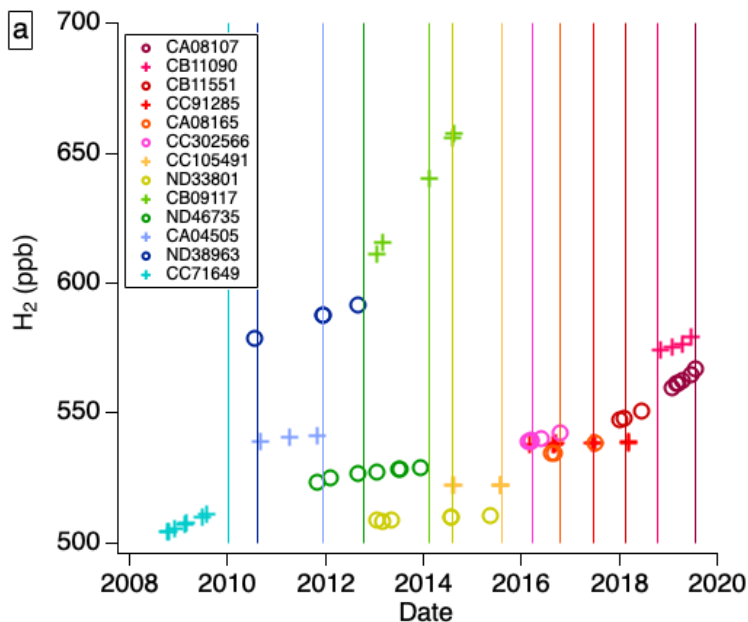
1239
1240



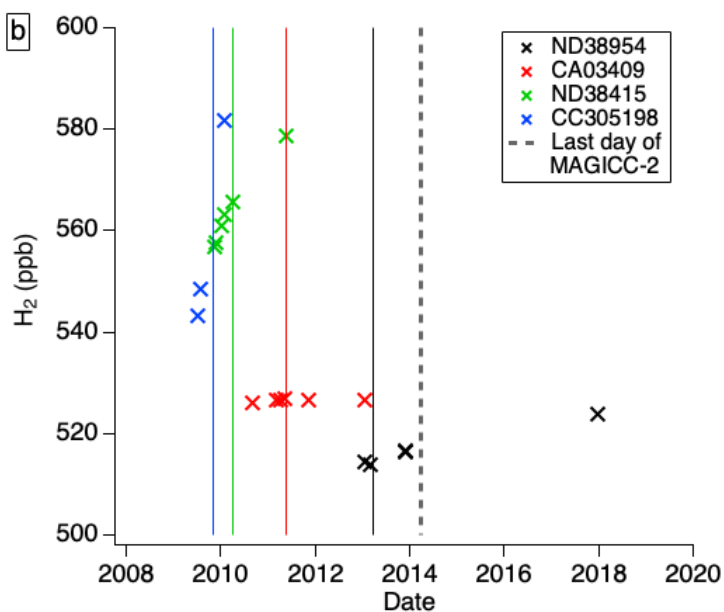
1241
1242
1243
1244
1245



1246 Figure 3. Calibration histories of a) MAGICC-1 / H11 and b) MAGICC-2 / H8 tertiary standards. The
1247 colored vertical line indicates when a standard started to be used.
1248



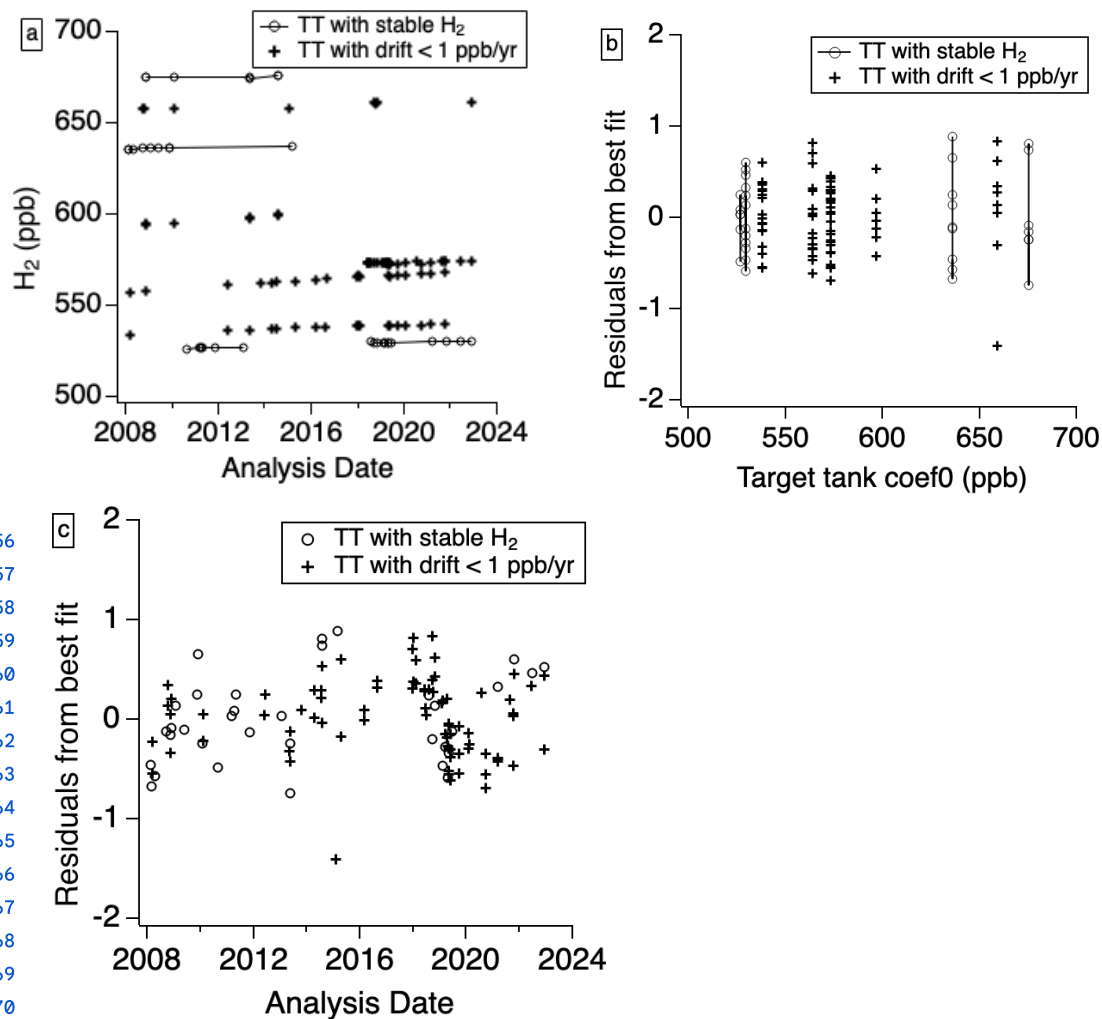
1249
1250
1251
1252



1253



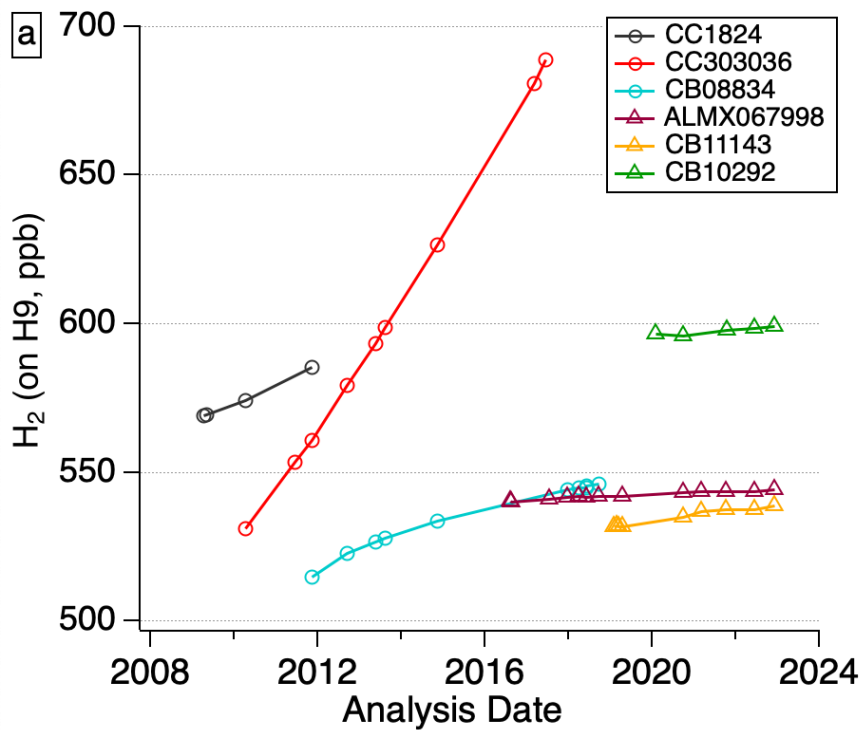
1254 Figure 4: Calibration histories and residuals to best fit for H9 target tanks with a stable H₂ mole fraction
1255 or a linear drift less than 1 ppb/yr. Residuals are in ppb.



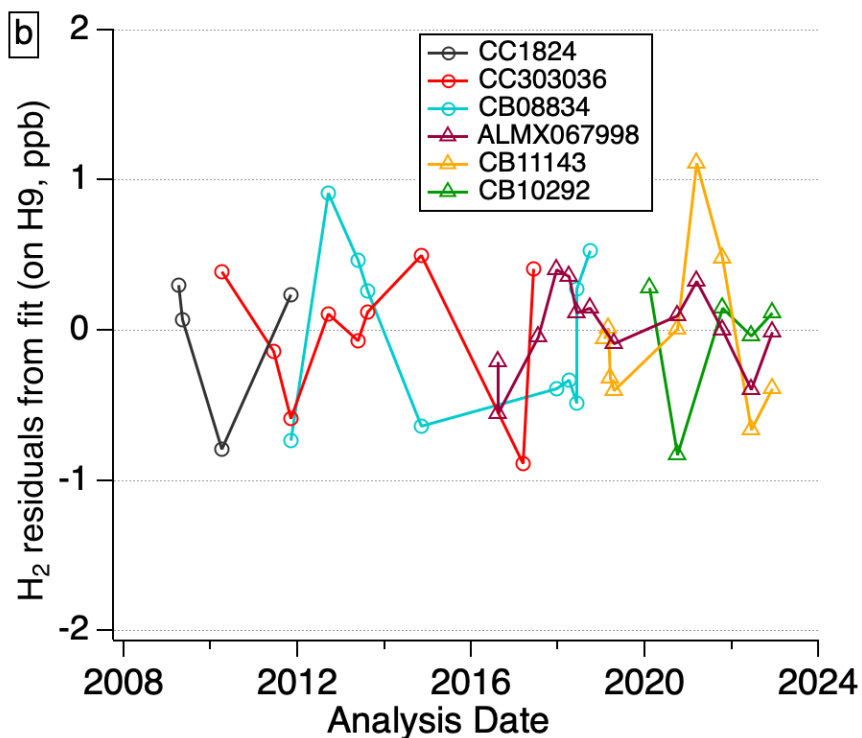
1256
1257
1258
1259
1260
1261
1262
1263
1264
1265
1266
1267
1268
1269
1270
1271
1272
1273
1274



1275 Figure 5. Flask air analysis system (H8 and H11) target air tanks H9 calibration histories and residuals to
1276 best linear or quadratic fit.
1277



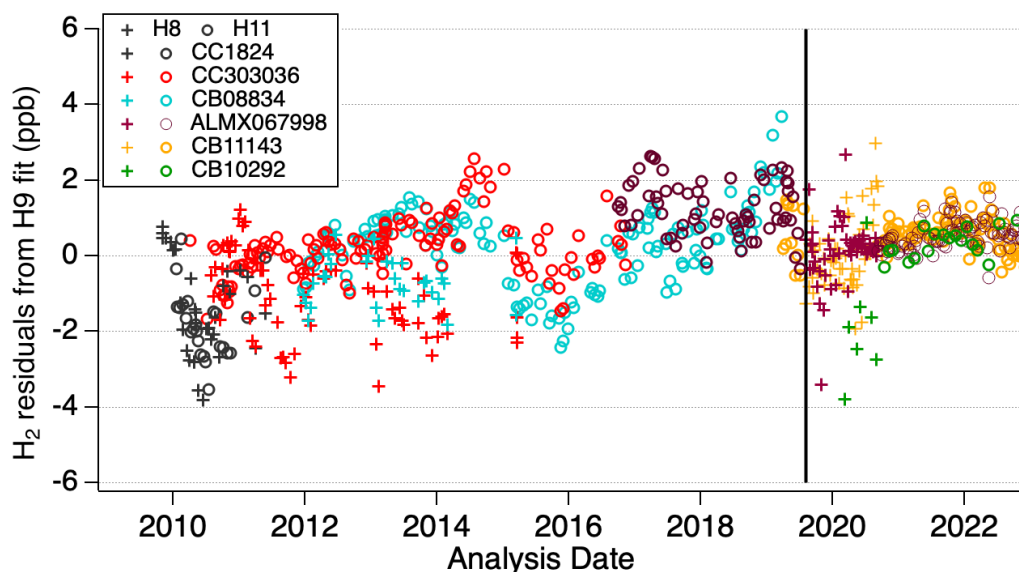
1278
1279



1280
1281
1282
1283
1284
1285
1286
1287
1288
1289
1290
1291
1292
1293
1294
1295
1296
1297
1298
1299
1300



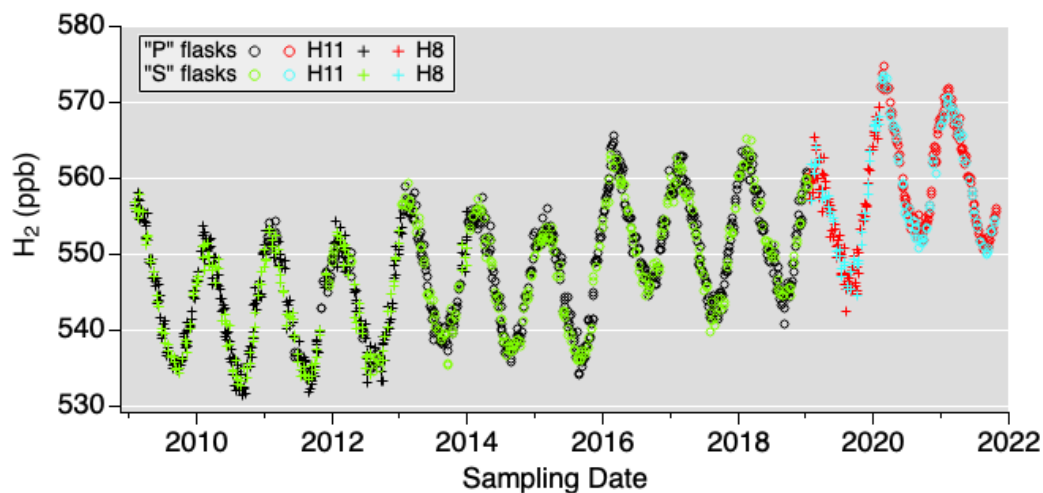
1301 Figure 6. Differences of target air tank H₂ analysis results on MAGICC and time-dependent assignment
1302 based on calibration history on H9. The vertical line indicates the transition to the MAGICC-3 flask
1303 analysis system.
1304



1305
1306
1307
1308
1309
1310
1311
1312

1307 Figure 7. South Pole Observatory flask air H₂ measurements. Circle and “+” symbols refer to instruments:
1308 H11 or H8. Black is used for measurements of P flasks on the MAGICC-1 or MAGICC-2 system and red
1309 for the MAGICC-3 system. Light green is used for measurements of S flasks on the MAGICC-1 or
1310 MAGICC-2 system and light blue for the MAGICC-3 system.

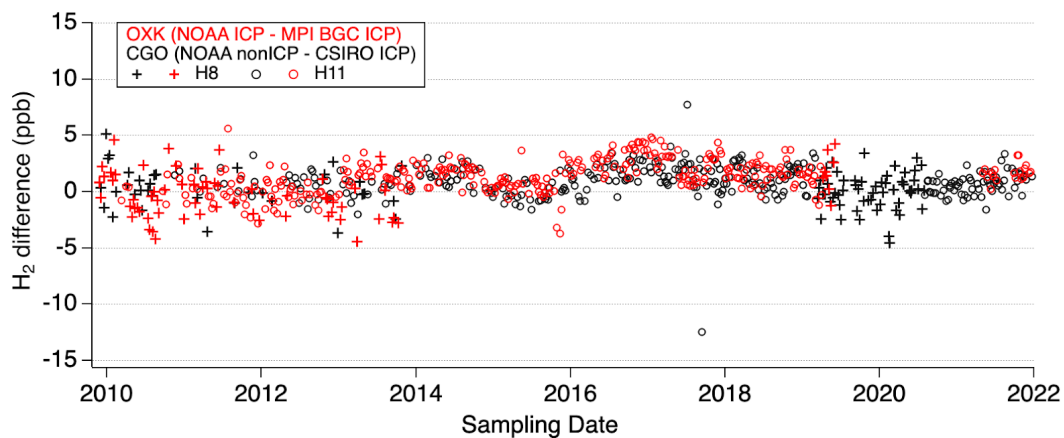
1311
1312



1313

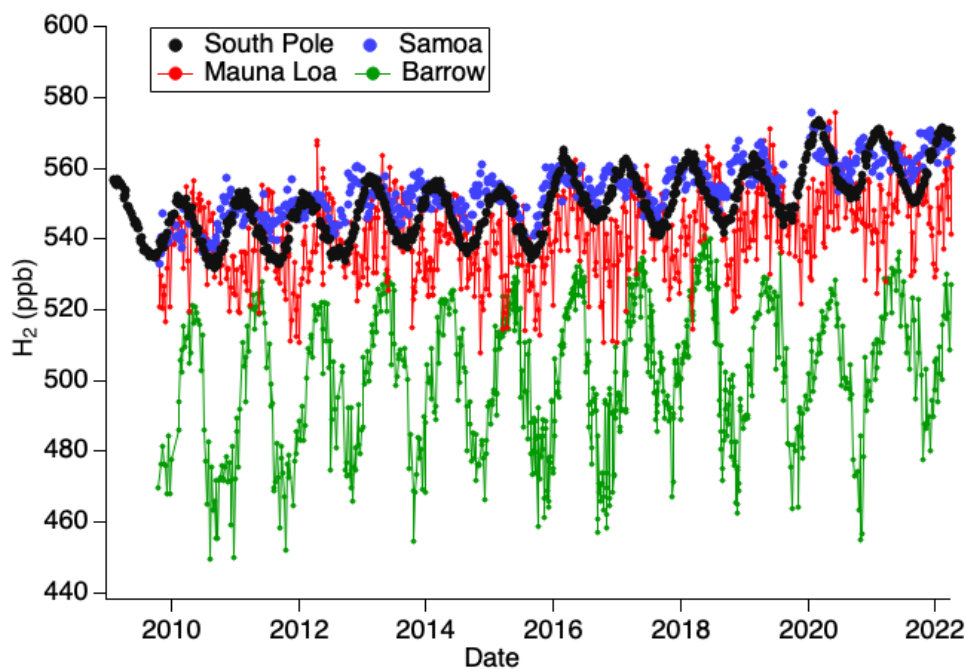


1314 Figure 8. Interlaboratory same air H₂ measurement difference for OXK ICP (NOAA - MPI BGC) and
1315 CGO (NOAA non ICP - CSIRO ICP).
1316



1317
1318
1319
1320
1321
1322

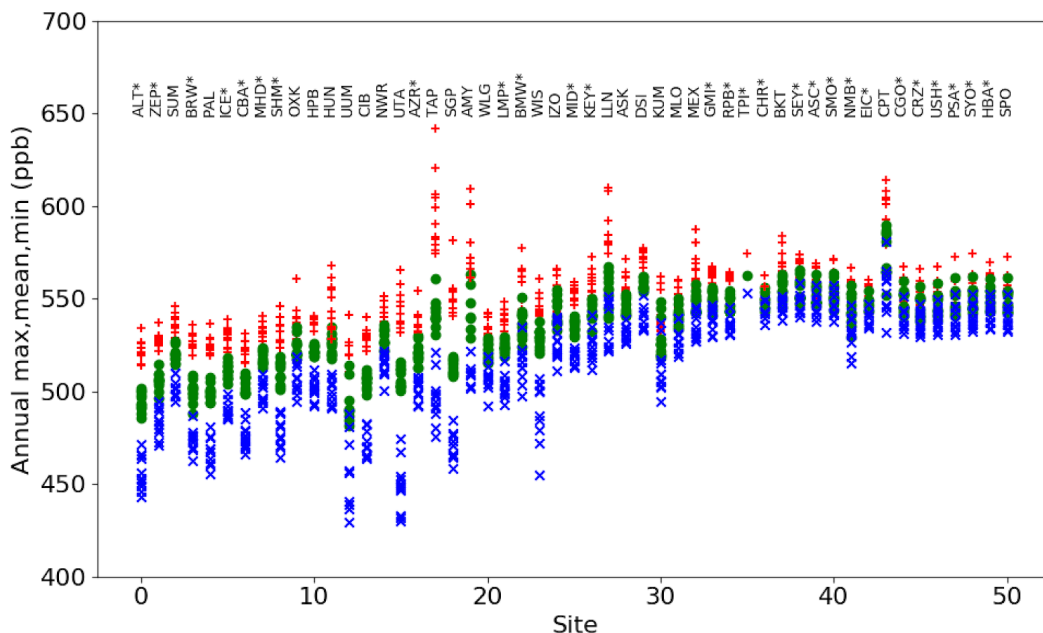
Figure 9. H₂ time series at the NOAA Baseline Atmospheric Observatories



1323
1324



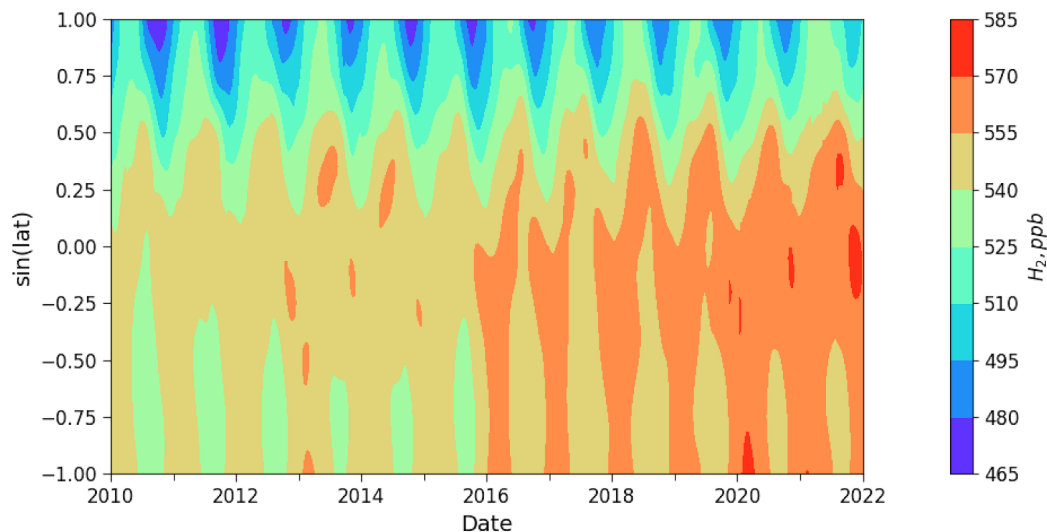
1325 Figure 10: Annual maximum (red), mean (green) and minimum (blue) H₂ from the smooth curve fit of the
1326 2010-2021 measurement time series for each surface site in the global sampling network. Each site is
1327 referred to with a three letter code (see details at <https://gml.noaa.gov/dv/site/>). The sampling sites are
1328 shown along the x-axis with decreasing latitudes. An asterisk near the site code indicates if the site data is
1329 used for the marine boundary layer air zonal and global means data reduction.
1330



1331
1332
1333
1334
1335
1336
1337
1338
1339
1340
1341
1342
1343
1344
1345
1346
1347
1348
1349



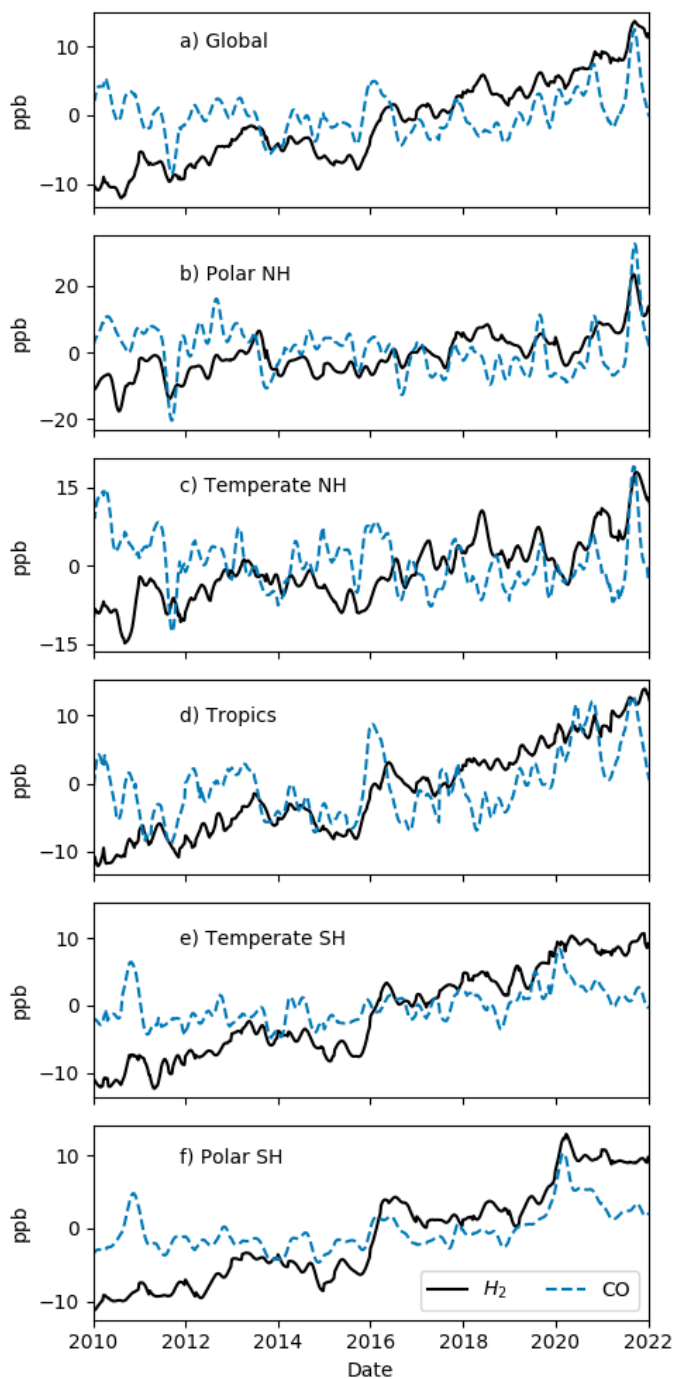
1350 Figure 11: 2010-2021 marine boundary layer H_2 meridional gradient. Y-axis is the sine of latitude.
1351



1352
1353
1354
1355
1356



1357 Figure 12: 2010-2021 marine boundary layer global and zonal mean H_2 anomaly (black line) and CO
1358 anomaly (dashed blue line) time series.



1359